Click Here for Full Article

A permanent El Niño–like state during the Pliocene?

Alan M. Haywood,[1,2] Paul J. Valdes,[3] and Victoria L. Peck[1]

Received 18 May 2006; revised 1 September 2006; accepted 20 October 2006; published 27 February 2007.

[1] The Pliocene may have been characterized by permanent El Niño–like conditions. Initial modeling studies suggest that this may have contributed to Pliocene warmth. The termination of this state may have influenced Northern Hemisphere glaciation (NHG). We use the Hadley Centre Coupled Model version 3 to examine the role of the oceans and ocean structure on Pliocene warmth. A permanent El Niño–like state is not predicted. Annual mean sea surface temperatures in the eastern equatorial Pacific at Ocean Drilling Program Sites 847 and 851 increase by 1.71°C and 1.15°C, respectively. However, El Niño Southern Oscillation events are clearly expressed by the model. Sensitivity tests indicate that a prescribed permanent El Niño–like condition increases annual global mean surface temperatures by a maximum of 0.6°C. If the Pliocene was characterized by such a condition, it is questionable that it provided a major contribution to global warmth and therefore unlikely that the termination of this state contributed significantly to the onset of NHG.

Citation: Haywood, A. M., P. J. Valdes, and V. L. Peck (2007), A permanent El Niño–like state during the Pliocene?, *Paleoceanography*, *22*, PA1213, doi:10.1029/2006PA001323.

1. Introduction

[2] The Pliocene has been the subject of intense study for the last two decades. There are many reasons for this, but the most important driver has been our desire to understand the dynamics of past warm climates as a potential guide to understanding climate change in the future.

[3] Potential causes of Pliocene warmth have been widely discussed [e.g., *Raymo et al.*, 1996] and can be summarized as relating to (1) paleogeographic change, e.g., altered elevations of major mountain chains such as the western cordillera of North and South America [*Rind and Chandler* 1991]; (2) altered atmospheric trace gas concentrations and water vapor content [e.g., *Van der Burgh et al.*, 1993; *Raymo and Rau*, 1992; *Haywood et al.*, 2005]; (3) changes to ocean circulation [*Ravelo and Andreasen*, 2000; *Cane and Molnar*, 2001], ocean heat transport [e.g., *Dowsett et al.*, 1992; *Haug and Tiedemann*, 1998; *Kim and Crowley*, 2000], or the thermal structure of the oceans [e.g., *Wara et al.*, 2005; *Philander and Fedorov*, 2003]; and (4) feedbacks generated through reduced land ice cover, surface albedo, cloud cover and temperature [*Haywood and Valdes*, 2004].

[4] Recent work has suggested that El Niño might have been a perennial rather than intermittent phenomenon during the Pliocene, and that sea surface temperatures (SSTs) in low latitudes were essentially independent of longitude [*Molnar and Cane*, 2002; *Philander and Fedorov* 2003; *Ravelo et al.*, 2004; *Wara et al.*, 2005; *Barreiro et al.*, 2005; *Ravelo et al.*, 2006]. *Barreiro et al.* [2005] use this state as a boundary condition for an atmospheric GCM, and in doing so find that the trade winds along the equator, and hence the Walker Circulation, collapse. Low-level stratus clouds in low latitudes diminish greatly, reducing the albedo of the Earth and increasing surface temperature. The atmospheric concentration of water vapor also increases, further contributing to global warming.

[5] *Philander and Fedorov* [2003] state that the global cooling, which led to the appearance of continental glaciers in high northern latitudes after 3 Myr ago, might have affected the thermal structure of the ocean by causing a gradual shoaling of the thermocline. They argue that when the thermocline became sufficiently shallow, winds were able to bring cold water from below the thermocline to the surface in upwelling regions which brought into play feedbacks involving ocean-atmosphere interactions of the type associated with ENSO (El Niño Southern Oscillation) and also mechanisms by which high-latitude surface conditions can influence the depth of the tropical thermocline. Because of the large area of tropics, any tropical changes could now affect the globally averaged surface temperature by influencing the Earth's cloud cover, albedo, and concentration of the water vapor. *Philander and Fedorov* [2003] suggest that the transition from uniformly warm tropics to the tropics with zonal SST gradients may have provided important positive feedbacks for the amplification of the glacial cycles and Northern Hemisphere glaciation (NHG).

[6] *Rickaby and Halloran* [2005] provide an alternative view of Pliocene tropical Pacific SSTs by reconstructing La Niña rather than El Niño–like conditions for the Pliocene based on Mg/Ca analyses of planktonic formainifera from the same Ocean Drilling Programme (ODP) sites used by *Wara et al.* [2005] study. *Rickaby and Halloran* [2005] propose that an ocean thermostat mechanism can explain how greenhouse gas heating of the tropical Pacific leads to a cooling in the eastern equatorial Pacific (EEP), arising from the different SST response in the EEP and the western equatorial Pacific (WEP). They argue that in the west, where the thermocline is deep, the SST rises thermo-

[1]Geological Sciences Division, British Antarctic Survey, Cambridge, UK.
[2]Now at School of Earth and Environment, University of Leeds, Leeds, UK.
[3]School of Geographical Sciences, University of Bristol, Bristol, UK.

Copyright 2007 by the American Geophysical Union.
0883-8305/07/2006PA001323$12.00

dynamically to attain a new equilibrium. In the east, where the thermocline is shallow, dynamic upwelling of cold waters counteracts the warming tendency. SST's increase more in the west than in the east, enhancing the zonal temperature gradient. As a consequence trade winds increase, which increases upwelling and thermocline tilt, cooling the surface waters in the east and further enhancing the temperature contrast [*Rickaby and Halloran*, 2005].

[7] We have performed a series of experiments using the Hadley Centre GCM examining the role of the oceans and ocean structure on mid-Pliocene warmth (2.97 to 3.29 Ma BP; see section 2.3 for more details). Firstly, we present results from a fully coupled mid-Pliocene ocean-atmosphere GCM simulation which examines the thermal structure of tropical oceans and longitudinal temperature gradients in the Pacific and other ocean basins, with the objective of identifying if the mid-Pliocene was indeed a period characterized by either a permanent El Niño–like or La Niña–like condition. Secondly, we present results from three sensitivity experiments where the gradient of SSTs in the tropical Pacific and other ocean basins is altered so that the influence of tropical ocean conditions on high-latitude precipitation and temperature estimates, and therefore indirectly NHG, can be quantified.

[8] The principal difference between this work and previous modeling studies is that we use a fully coupled ocean-atmosphere GCM running with a full suite of boundary conditions appropriate for the mid-Pliocene. Our aim is to examine (1) whether or not our model is capable of predicting, rather than being prescribed with, permanent El Niño–like or La Niña–like conditions for the mid-Pliocene and to examine what significance this has to mid-Pliocene warmth and (2) what the effect on the coupled ocean-atmosphere system is of prescribing a permanent El Niño–like state.

2. Methods

2.1. Coupled Ocean-Atmosphere Modeling for the Pliocene

[9] The particulars of the version of the UKMO GCM (hereinafter referred to as HadCM3) used in this study are well documented [*Gordon et al.*, 2000]. In brief, HadCM3 was developed at the Hadley Centre for Climate Prediction and Research, which is a part of the UK Meteorological Office. The model requires no flux corrections to be made, even for simulations of a thousand years or more [*Gregory and Mitchell*, 1997]. The GCM consists of a linked atmospheric model, ocean model and sea ice model. The horizontal resolution of the atmospheric model is 2.5° in latitude by 3.75° in longitude. This gives a grid spacing at the equator of 278 km in the north-south direction and 417 km east-west and is approximately comparable to a T42 spectral model resolution. The atmospheric model consists of 19 layers. The spatial resolution over the ocean in HadCM3 to 1.25° × 1.25° and the model has 20 layers. The atmospheric model has a time step of 30 minutes and includes a radiation scheme that can represent the effects of minor trace gases [*Edwards and Slingo*, 1996]. A parameterization of simple background aerosol climatology is also included [*Cusack et al.*, 1998]. The convection scheme used is that of *Gregory et al.* [1997]. A land-surface scheme includes the representation of the freezing and melting of soil moisture. The representation of evaporation includes the dependence of stomatal resistance on temperature, vapor pressure and CO_2 concentration [*Cox et al.*, 1999].

[10] The ocean model uses the Gent-McWilliams mixing scheme [*Gent and McWilliams*, 1990]. There is no explicit horizontal tracer diffusion in the model. The horizontal resolution allows the use of a smaller coefficient of horizontal momentum viscosity, compared to HadCM2, leading to an improved simulation of ocean velocities. The sea ice model uses a simple thermodynamic scheme and contains parameterizations of ice drift and leads [*Cattle and Crossley*, 1995].

2.2. Experimental Design

[11] Our starting point is a fully coupled ocean-atmosphere simulation for the preindustrial and the mid-Pliocene. Our mid-Pliocene control experiment (hereinafter referred to as $\text{Plio}^{\text{Control}}$) was set up with mid-Pliocene boundary conditions derived from the USGS PRISM2 data set (see next section for further details) and represents a continuation of the simulation described by *Haywood and Valdes* [2004]. *Haywood and Valdes* [2004] provide a detailed discussion of the simulated ocean and atmospheric state for the mid-Pliocene, as well as a comprehensive evaluation of the model results to proxy data. The study concluded that there was no increase in meridional ocean heat transport and that Atlantic thermohaline circulation decreased by ~3 Sv. The model appeared to significantly underestimate the changes in SSTs in the North Pacific and North Atlantic and overestimate SST changes in the tropics, compared to faunal analysis SST data [*Dowsett et al.*, 1999]. However, the discrepancy in the tropics was resolved when model outputs were compared to alkenone-based tropical SST estimates [*Haywood et al.*, 2005]. For more details the reader is referred to *Haywood and Valdes* [2004] and *Haywood et al.* [2005].

[12] The studies referred to above did not address ENSO variability during the mid-Pliocene. Therefore we have conducted an analysis of ENSO variability in experiment $\text{Plio}^{\text{Control}}$, and related changes to ocean thermal structure in the tropics. This analysis was performed to identify whether or not a permanent El Niño–like or La Niña condition exited in the model simulation. We also present results from three mid-Pliocene sensitivity experiments (hereinafter referred to as $\text{PlioPacific}^{\text{NoGradient}}$, $\text{PlioPacific}^{\text{Dateline}}$ and $\text{PlioGlobal}^{\text{Dateline}}$) where the gradient of SSTs in the tropical Pacific and other ocean basins is altered, so that the influence of tropical ocean conditions on high-latitude precipitation and temperatures estimates, and therefore indirectly NHG, can be quantified.

[13] In experiment $\text{PlioPacific}^{\text{NoGradient}}$ all boundary and initial conditions were kept the same as $\text{Plio}^{\text{Control}}$ except that a strong Haney restoring function (14 day timescale) was used, between 40° north and south of the equator, to relax Pacific SST to a value appropriate to the western Pacific warm pool, in effect extending western Pacific warm pool SSTs across the entire Pacific. In experiment

Table 1. Details of Trace Gas Concentrations for All Model Experiments, Length of Model Simulations, the Period Used to Calculate Climatological Means, the Model-Predicted Radiation Balance at the Top of the Atmosphere, and Predicted Global Annual Mean Surface Temperatures (Including Change From Preindustrial)

Model Experiment	CO_2, ppm	CH_4, ppb	NO_2, ppb	$CFC^{11}$and CFC^{12}, ppt	Radiation Balance at the Top of the Atmosphere, W m^{-2}	Length of Model Run, years	Climatological Means	Global Annual Average Surface Temperature, °C	ΔT, °C
Pre-Ind	279	703	276	0	−0.39	500	last 60 years	14.17	-
$Plio^{Control}$	400	703	276	0	0.25	400	last 60 years	17.1	2.93
$PlioPacific^{NoGradient}$	400	703	276	0	−0.62	400 ($Plio^{Control}$) + 120	last 60 years	17.77	3.6
$PlioPacific^{Dateline}$	400	703	276	0	0.91	400 ($Plio^{Control}$) + 120	last 60 years	17.11	2.94
$PlioGlobal^{Dateline}$	400	703	276	0	0.89	400 ($Plio^{Control}$) + 120	last 60 years	17.12	2.95

$PlioPacific^{Dateline}$, Pacific SSTs between 40° north and south were relaxed using a Haney restoring function to SSTs at the dateline rather than the western Pacific warm pool. In experiment $PlioGlobal^{Dateline}$ SSTs were relaxed to dateline values across the Atlantic and Indian Oceans as well as the Pacific Ocean between 40° north and south of the equator.

[14] A CO_2 concentration of 400 ppmv is used in all mid-Pliocene coupled ocean-atmosphere experiments. This is a justifiable value when available proxy estimates of Pliocene atmospheric CO_2 concentrations are considered. Estimates have been derived from the analysis of stomatal density of fossil leaves [*Van der Burgh et al.*, 1993; *Kürschner et al.*, 1996], through analyses of $\delta^{13}C$ ratios of marine organic carbon [*Raymo and Rau*, 1992; *Raymo et al.*, 1996] and through measurement of the differences between the carbon isotope composition of surface and deep waters [*Shackleton et al.*, 1992]. All three proxy methods suggest that absolute CO_2 levels during the time period range from 360 to 400 ppmv, compared to mid-19th century levels of approximately 280 ppmv and modern concentrations of 378 ppmv. For further details of the experimental design see Table 1.

[15] The Pre-Ind and $Plio^{Control}$ simulations were integrated for 500 and 400 years, respectively. Experiments $PlioPacific^{NoGradient}$, $PlioPacific^{Dateline}$ and $PlioGlobal^{Dateline}$ represent continuation runs of experiment $Plio^{Control}$ and were integrated for an additional 120 years. Climatological means were derived from the final 60 simulated years in all cases. An analysis of the model's energy imbalance at the top of the atmosphere (TOA) for all experiments is presented in Table 1. For all experiments there is no observable trend in surface temperatures. Therefore we consider that all of the model runs have reached a quasi-equilibrium state.

2.3. Mid-Pliocene Boundary Conditions

[16] Required boundary conditions were supplied by the United States Geological Survey (USGS) PRISM2 2° × 2° digital data set. The particulars of the PRISM2 data set have been well documented in previous papers [*Dowsett et al.*, 1999; *Haywood et al.*, 2000, and references therein]. In brief, the prescribed boundary conditions cover the time slab between 3.29 and 2.97 Ma BP according to the geomagnetic polarity time scale [*Berggren et al.*, 1995]. Boundary conditions integrated into the model that are specific to the Pliocene include: (1) continental configuration, modified by a 25 m increase in global sea level, (2) modified present-day elevations, (3) reduced ice sheet size and height for Greenland (∼50% reduction) and Antarctica (∼33% reduction) and (4) Pliocene vegetation distribution. In addition Pliocene SSTs and sea ice distributions are provided in PRISM2 and were used to Haney force the model in the first 30 years of experiment $Plio^{Control}$ only.

[17] The geographical extent of the Greenland and Antarctic Ice Sheets within the PRISM2 data set was based on global sea level estimates derived for the Pliocene by *Dowsett and Cronin* [1990]. The PRISM2 reconstruction uses model results from M. Prentice (personal communication, 1999, cited by *Dowsett et al.* [1999]) to guide the areal and topographic distribution of Antarctic and Greenland ice. A 25 m sea level rise is equivalent to a maximum decrease in global average salinity of approximately 0.25 practical salinity unit (psu), which is small and therefore was not included in our Pliocene coupled simulations. For a more detailed description of the PRISM2 data set and how it differs from earlier PRISM data sets, see *Dowsett et al.* [1999] (available at http://pubs.usgs.gov/of/1999/of99-535/).

2.4. Challenges in Modeling ENSO

[18] Because of the importance of ENSO to ecology, society and economics, the ability of climate models to predict ENSO, to reproduce events in different models, and the changes in the magnitude of ENSO due to greenhouse gas emissions in different GCMs (including HadCM3) has been investigated in detail.

[19] *Brown et al.* [2006] summarize the ability of the HadCM3 GCM to simulate the mean state as well ENSO variability in the tropical Pacific. HadCM3 has a known cool bias in the central equatorial Pacific Ocean and a warm bias over the maritime continent. The equatorial Pacific trade winds are stronger than observed, and convection tends to be confined to the western Pacific Warm Pool and is stronger than observed. Overall, ENSO is simulated in HadCM3 as well as other coupled ocean-atmosphere model, with an amplitude and frequency that is broadly similar to observations.

[20] *Joseph and Nigam* [2006] examined ENSO teleconnections in a range of climate models. They conclude that spatial and temporal structure of monthly SST anomalies is on the whole well modeled by HadCM3, but room for improvement remains particularly in the western Pacific. Similarly, precipitation teleconnections over the tropical Pacific and North America are realistic in HadCM3 but the surface air temperature linkages are not as well represented. *Turner* [2004] shows that the teleconnections between ENSO and the Southern Hemisphere are also reasonably simulated within HadCM3.

[21] The model dependency of our results is an important aspect to consider. However, we are the first to publish a fully coupled ocean-atmosphere GCM simulation for the Pliocene. Therefore it is very difficult for us to directly quantify the potential importance of model dependency on our results. Other studies using different versions of the Hadley Centre model for modern and future climate change scenarios are available and are relevant in this context. For example, *Collins* [2000a], using version 2 of the Hadley Centre Coupled Model (HadCM2), found that at four times preindustrial levels of CO_2 ENSO events became larger in amplitude and more frequent than present day ENSO events. Thus in addition to the impacts of climate change, the impacts of ENSO events would be felt more often and with greater magnitude. However, using version 3 of the Hadley Centre Coupled Model (HadCM3), *Collins* [2000b] found that magnitude and frequency of ENSO events remained unchanged as greenhouse gases increased. The range of uncertainty in the future behavior of ENSO is increased when one examines the responses of other AOGCMs [*Cubash et al.*, 2001; *Collins and CMIP Modelling Groups*, 2005].

[22] *Collins* [2000b] attributed the difference in the ENSO response to global warming between HadCM2 and HadCM3 to differences in the response of the mean climate of the two models in the tropical Pacific region, since forcing HadCM3 with the pattern of mean SST warming from HadCM2 caused the HadCM3 ENSO cycle to amplify and to become more frequent, much like the HadCM2 ENSO response. *Collins* [2000b] links the differences in the pattern of mean climate change between HadCM2 and HadCM3 to the fact that the ocean component in HadCM3 has a higher resolution than the equivalent component in HadCM2. Also HadCM3 does not require a flux adjustment term to control climate drift [*Johns et al.*, 1997; *Gordon et al.*, 2000]. However, *Williams et al.* [2001] examined changes in the physical parameterizations of cloud formation and the representation of atmospheric boundary layer processes between HadCM2 and HadCM3 and found that small changes to these schemes could combine in a nonlinear way to produce the large differences in the patterns of cloud, precipitation and SST change in the two models. Cloud feedbacks are among the most important and most complex of feedbacks in the climate system and it appears that even small perturbations to the parameters of cloud models can cause nonlinear and far-reaching differences in global climate change [*Collins*, 2000b; *Williams et al.*, 2001].

[23] Similarly, a comparison of PMIPII (Palaeoclimate Modelling Intercomparison Project) mid Holocene simulations (6 Ka) showed that the majority of models predicted a weakening of ENSO variability (in agreement with proxy data), but the magnitude of decrease varied considerably between models. Results derived from HadCM3 fall in the middle of the PMIPII range (P. J. Valdes, unpublished data, 2006).

[24] The uncertainty in the ability of the HadCM3 GCM to simulate ENSO variability obviously has implications for our work. However, it has been established that HadCM3 is relatively sensitive in terms of predicting ENSO events [*Achutarao and Sperber*, 2002]. In a CMIP (Coupled Model Intercomparison Project) ensemble of flux adjusted and non flux adjusted models, HadCM3 performed consistently well against observational data, capturing the variability in tropical Pacific surface air temperatures as well as simulating correctly the timing of the annual cycle of Pacific SSTs and the amplitude of recent ENSO events [*Achutarao and Sperber*, 2002]. Therefore we feel justified in using HadCM3 as a tool for investigating Pliocene ENSO and high-latitude teleconnections.

2.5. Diagnostic Predictions of $\delta^{18}O_{sw}$

[25] A similarity between the $\delta^{18}O$ signal in planktonic foraminifera from the EEP and WEP prior to 2.5 Ma BP has been used as one line of evidence to support the premise that the SST gradient was reduced during the Pliocene [e.g., *Ravelo et al.*, 2004]. An important consideration in calculating paleo-SSTs using the $\delta^{18}O$ signal from planktonic foraminifer is the $\delta^{18}O$ value of seawater ($\delta^{18}O_{sw}$). The local or regional surface $\delta^{18}O_{sw}$ is a function of the global mean composition as well as geographical variations caused by the combined effects of changes in evaporation-precipitation patterns, runoff (in coastal regions), and ocean circulation patterns [*Zachos et al.*, 1994; *Schmidt*, 1998]. To assess the relative importance of temperature versus salinity changes on the $\delta^{18}O_{sw}$ signal for the Pliocene we present diagnostic $\delta^{18}O_{sw}$ predictions based on our paleoclimate modeling studies.

[26] Model calculated values for the $\delta^{18}O$ of seawater are an attempt to capture longitudinal and latitudinal change as a function of climate, and are based on precipitation minus evaporation (P − E) estimates derived from the GCM. Present-day observed $\delta^{18}O_{sw}$ [*Bigg and Rohling*, 2000; *Schmidt*, 1999; G. A. Schmidt et al., 1999, Global seawater oxygen-18 database, available at http://data.giss.nasa.gov/o18data/] is calibrated against observed P − E (ECMWF reanalysis data) for the Pacific and Atlantic Ocean basins. The resulting formulae (see below) are used to predict $\delta^{18}O_{sw}$ gradients for the Pliocene.

Atlantic Calibration

$$\delta^{18}O_{sw} = 0.24 - 0.008(P - E) \qquad r^2 = 0.7 \qquad (1)$$

Pacific Calibration

$$\delta^{18}O_{sw} = 0.23 - 0.00004(P - E) \qquad r^2 = 0.4 \qquad (2)$$

P − E is given in units of cm yr^{-1}.

[27] By performing these diagnostics we can estimate how much of the $\delta^{18}O$ signal in planktonic foraminifera from the tropical Pacific could be attributable to salinity differences rather than alterations in SSTs. Although this is a useful approach, care must be taken when examining the results since they are based solely on the models predictions of P − E, where in reality the $\delta^{18}O_{sw}$ is also dependant upon mixing because of ocean currents, runoff, etc. Also, as can be seen in equation (2), the resulting correlation for the Pacific Ocean $\delta^{18}O_{sw}$ to P − E is relatively weak but significantly stronger for the Atlantic Ocean (see equation (1)). In addition to P − E we have also calibrated

$\delta^{18}O_{sw}$ against salinity [*Levitus and Boyer*, 1994]. This increased the r^2 value to 0.9 for both Atlantic and Pacific Oceans but did not significantly change the diagnostic predictions of $\delta^{18}O_{sw}$ generated using P − E. Nevertheless, it is important to recognize that the use of a salinity:$\delta^{18}O$ or P − E:$\delta^{18}O$ covariation from present-day observations as a diagnostic for the $\delta^{18}O$ composition of seawater during the mid-Pliocene is complicated by the fact that temperature gradients are steeper today then they were during the Pliocene (a reflection of cooler temperatures in polar regions today) which will result in different patterns of Rayleigh distillation and hence different $\delta^{18}O$ values in the hydrological cycle [*Rohling and Bigg*, 1998; *Rohling*, 2000]. Whilst this may lead to errors in individual $\delta^{18}O_{sw}$ values for specific locations, predicted changes in spatial gradients in a single ocean basin are likely to be more robust.

3. Results

3.1. Surface Temperature (°C)

[28] The annual mean surface temperature in experiment $Plio^{Control}$ is ~3 °C higher than in experiment Pre-Ind (Table 1). The most significant warming occurs in the high latitudes during the winter season in both hemispheres (Figure 1). A surface temperature increase of 15°C or more is not uncommon over Antarctic and temperatures over Greenland increase by ~8°C. This change is related to the reduced extent of land ice cover specified in the PRISM2 data set and used as a model boundary condition. Surface temperatures warm significantly (~1 to 8°C) over North and South America, Africa, Eurasia and Australia. The warming in North America and Eurasia is particular pronounced during December, January and February (DJF). Surface temperatures over the oceans warm in most areas. However, this is amplified at the higher latitudes because of a reduction in the coverage of sea ice. Tropical Pacific temperatures rise by 1 to 5°C. This change is predicted in both the EEP and WEP (Figure 1).

[29] In sensitivity experiments $PlioPacific^{NoGradient}$, $PlioPacific^{Dateline}$ and $PlioGlobal^{Dateline}$, surface temperatures in the central Pacific, and particularly the EEP, are warmer than experiment $Plio^{Control}$ (Figure 1). During DJF there is a substantial warming over North America in all of the sensitivity experiments, associated with Rossby Wave propagation (see section 3.6). In experiments $PlioPacific^{Dateline}$ and $PlioGlobal^{Dateline}$ there is also a substantial cooling over Greenland and the Arctic. Warming (~1°C) is predicted in both seasons over tropical Africa and is associated with changes in tropical atmospheric circulation. In the mid and high latitudes of the Southern Hemisphere, winter (June, July and August (JJA)) temperatures decrease by 1 to 6°C (Figure 1). Cooling over the Southern Ocean is associated with an increase in the percentage coverage (10 to 20% increase in the fractional coverage) of sea ice in all of the sensitivity experiments, and also a reduction in ocean mixed layer depth (~50 m). The cooling in the Antarctic is more clearly expressed in experiments $PlioPacific^{Dateline}$ and $PlioGlobal^{Dateline}$. $PlioPacific^{NoGradient}$ global annual mean surface temperature is ~0.6°C higher than experiment $Plio^{Control}$. Global annual mean surface temperatures in experiments $PlioPacific^{Dateline}$ and $PlioGlobal^{Dateline}$ are the same as experiment $Plio^{Control}$ (Table 1) because of a cancellation effect between tropical warming and high-latitude cooling.

3.2. Pacific Ocean Temperatures (°C) and Ocean Salinity (psu)

[30] $Plio^{Control}$ annual mean ocean temperatures, as a profile across the Pacific Ocean at 0° north, demonstrate a clear gradient in the depth of the thermocline (Figure 2). In the WEP and the central Pacific the modeled thermocline depth is ~180 to 200 m. This shallows rapidly in the EEP so that the thermocline is near the surface. Pacific Ocean temperatures in experiment $Plio^{Control}$ are 1 to 3°C warmer (to a depth of more than 360 m) than experiment Pre-Ind. This warming is expressed in both the EEP and the WEP (Figure 2). The relaxation of SSTs to values equivalent to the WEP warm pool in experiment $PlioPacific^{NoGradient}$ increases central and EEP ocean temperatures in the top 60 m by 1 to more than 5°C. Ocean warming in experiment $PlioPacific^{Dateline}$ is primarily restricted to the EEP and, as one would expect, not as great as the warming predicted in experiment $PlioPacific^{NoGradient}$ (Figure 2).

[31] The main differences in surface ocean salinity between experiment $Plio^{Control}$ and Pre-Ind, as well as the three sensitivity experiments and experiment $Plio^{Control}$, track the variations in total precipitation rate predicted by the model. Experiment $Plio^{Control}$ shows a freshening (up to 1.2 psu) of the surface ocean in the central Pacific between 10° and 20° north (Figure 3). Areas of the EEP become more saline (by ~1 psu). The prescribed SSTs in experiments $PlioPacific^{NoGradient}$, $PlioPacific^{Dateline}$ and $PlioGlobal^{Dateline}$ generate large ocean salinity differences from experiment $Plio^{Control}$. The broad pattern of changes are similar but the changes in salinity gradients in experiments $PlioPacific^{Dateline}$ and $PlioGlobal^{Dateline}$ are less compared to experiment $PlioPacific^{NoGradient}$. Salinity decreases over a wide area of the WEP and Central Pacific (up to −2.6 psu) and increases (by 2.0 psu) in the EEP (Figure 3). A salinity increase between 0° and 30° north (1 to 2.6 psu) is observed across the Pacific Ocean in experiment $PlioPacific^{Dateline}$ and is matched by a freshening of surface waters of a similar magnitude across the Pacific between 0 and 25° south (Figure 3). Differences between experiments $PlioPacific^{NoGradient}$ and $PlioPacific^{Dateline}$ demonstrate the sensitivity of predicted salinity values to initial SSTs (Figure 3). This is related to changes in the hydrological cycle associated with the relatively cooler prescribed SSTs in experiment $PlioPacific^{Dateline}$.

3.3. Total Precipitation Rate (mm d^{-1})

[32] Seasonally, significant differences are predicted in the spatial distribution of precipitation between the $Plio^{Control}$ and Pre-Ind experiments. In the Northern Hemisphere, at middle-to-high latitudes, DJF precipitation rates increase by 0.5 to 3 mm d^{-1} (Figure 4). The increase in midlatitude precipitation is associated with enhanced surface temperatures predicted in the $Plio^{Control}$ experiment. This pattern in not mirrored in the Southern Hemisphere largely because of the lower magnitude of surface temperature change. DJF total precipitation rates decrease over

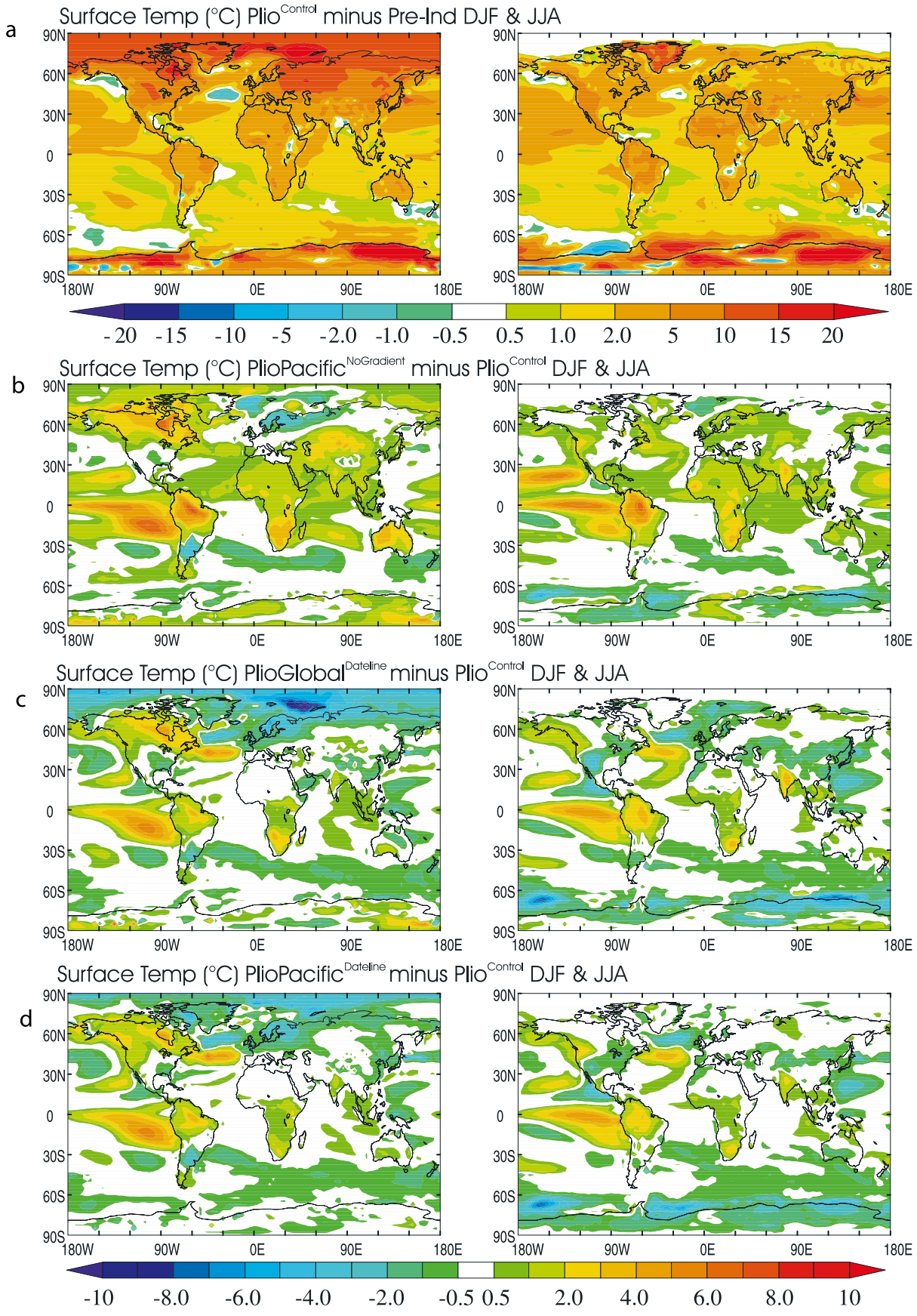
a
Surface Temp (°C) Plio^Control minus Pre-Ind DJF & JJA
b
Surface Temp (°C) PlioPacific^NoGradient minus Plio^Control DJF & JJA
c
Surface Temp (°C) PlioGlobal^Dateline minus Plio^Control DJF & JJA
d
Surface Temp (°C) PlioPacific^Dateline minus Plio^Control DJF & JJA
90N
60N
30N
0
30S
60S
90S
180W
90W
0E
90E
180E
-20 -15 -10 -5 -2.0 -1.0 -0.5 0.5 1.0 2.0 5 10 15 20
-10 -8.0 -6.0 -4.0 -2.0 -0.5 0.5 2.0 4.0 6.0 8.0 10

Figure 1

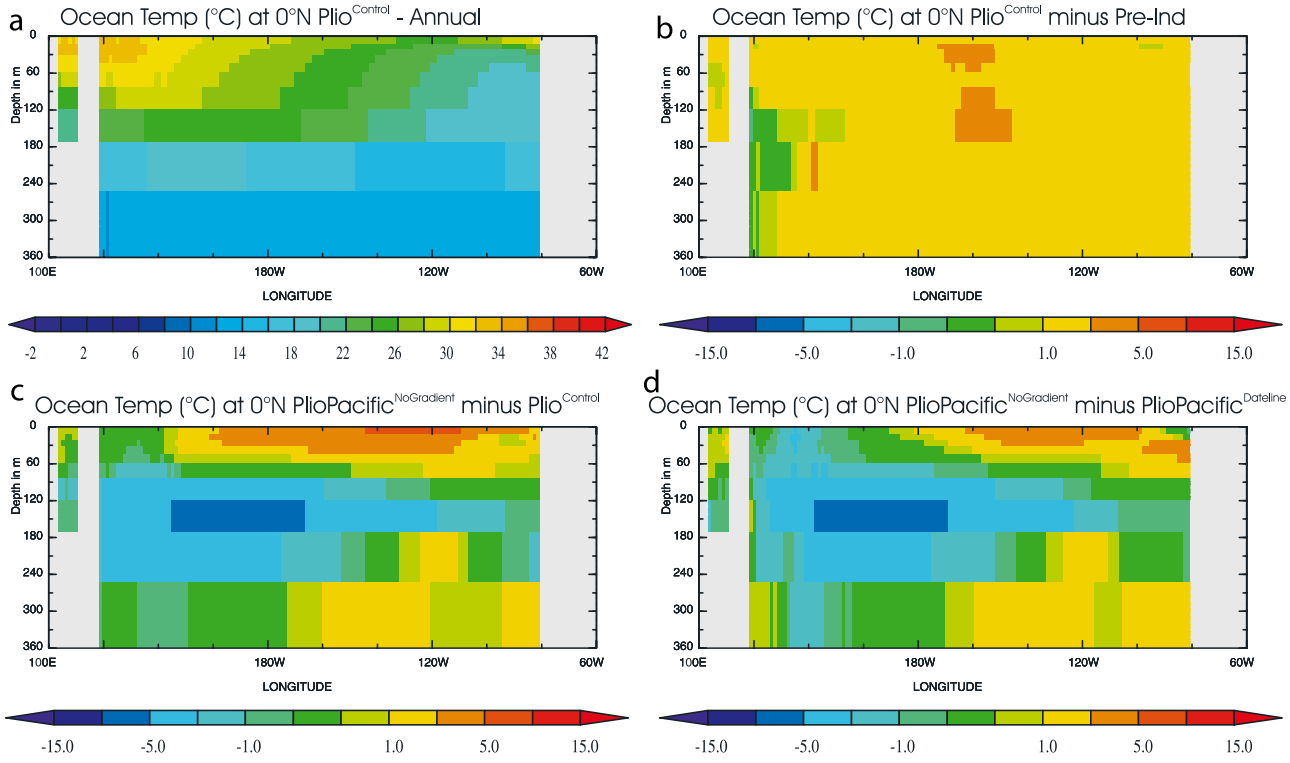

Figure 2. Profiles of annual mean ocean temperatures (°C) across the equatorial Pacific (at 0°N). (a) Absolute ocean temperatures for experiment Plio^{Control}. (Note the thermocline gradient across the Pacific.) (b) Difference in ocean temperature between experiments Plio^{Control} and Pre-Ind. (c) Difference in ocean temperatures between experiments PlioPacific^{NoGradient} and Plio^{Control}. (d) Difference in ocean temperatures between experiments PlioPacific^{NoGradient} and PlioPacific^{Dateline}.

areas of Southwest United States, the Atlantic and the western and eastern Mediterranean Basins (Figure 4). This latter change relates to a shift in the position of the winter storm track and associated enhancement of the Azores high-pressure system, which acts to block Atlantic depressions from entering the Mediterranean and instead diverts the precipitation across NW Europe. This pattern is akin in many respects to the North Atlantic Oscillation (NAO) in a positive phase. Total precipitation rates increase over parts of Southeast Asia during JJA, possibly indicative of an enhanced summer monsoon (Figure 4).

[33] In sensitivity experiments PlioPacific^{NoGradient}, PlioPacific^{Dateline} and PlioGlobal^{Dateline}, the altered gradient of SSTs across the Pacific and other ocean basins, and associated changes in the position of the Intertropical Convergence Zone (ITCZ), generate large variations in tropical precipitation rates (Figure 4). In the central Pacific, between 0° north and 10° south, total precipitation rate for both DJF and JJA increases by 0.5 to >10.0 mm d^{-1}. In the EEP this increase extends to nearly 30° south during DJF. Precipitation decreases by 0.5 to >10.0 mm d^{-1} across the Pacific between 0 and 10° north during DJF. This trend extends across to the tropical Atlantic. Precipitation rates increase over a wide area of the Indian Ocean during DJF and JJA whilst the signal in the WEP is more complex. JJA precipitation over India declines suggestive of a weaker (or geographically shifted) summer monsoon. Precipitation rate during DJF off the East cost of North America increases by 0.5 to 3 mm d^{-1}.

3.4. Tropical Pacific Surface Wind Stress (N m^{-2})

[34] Surface wind stress in an important part of the dynamics of ENSO, and a potential collapse of the Walker circulation is a central tenant of the argument presented by *Philander and Fedorov* [2003] and *Barreiro et al.* [2005] in support of a permanent El Niño–like state during the Pliocene. In order to investigate this within our Pliocene sensitivity experiments it is important to examine the changes in surface wind stress. Tropical Pacific surface wind stress for experiments, Pre-Ind, Plio^{Control}, PlioPacific^{NoGradient} and PlioPacific^{Dateline} during March April and May (MAM) and September, October and November (SON) is shown in Figure 5. The seasonal pattern of surface wind stress over the Pacific in experiment Plio^{Control} is very similar to experiment Pre-Ind. Because of

Figure 1. Surface temperature results (°C) for (left) DJF and (right) JJA. (a) Difference between experiments Plio^{Control} and Pre-Ind. (b) Difference between experiments PlioPacific^{NoGradient} and Plio^{Control}. (c) Difference between PlioGlobal^{Dateline} and Plio^{Control}. (d) Difference between PlioPacific^{Dateline} and Plio^{Control}.

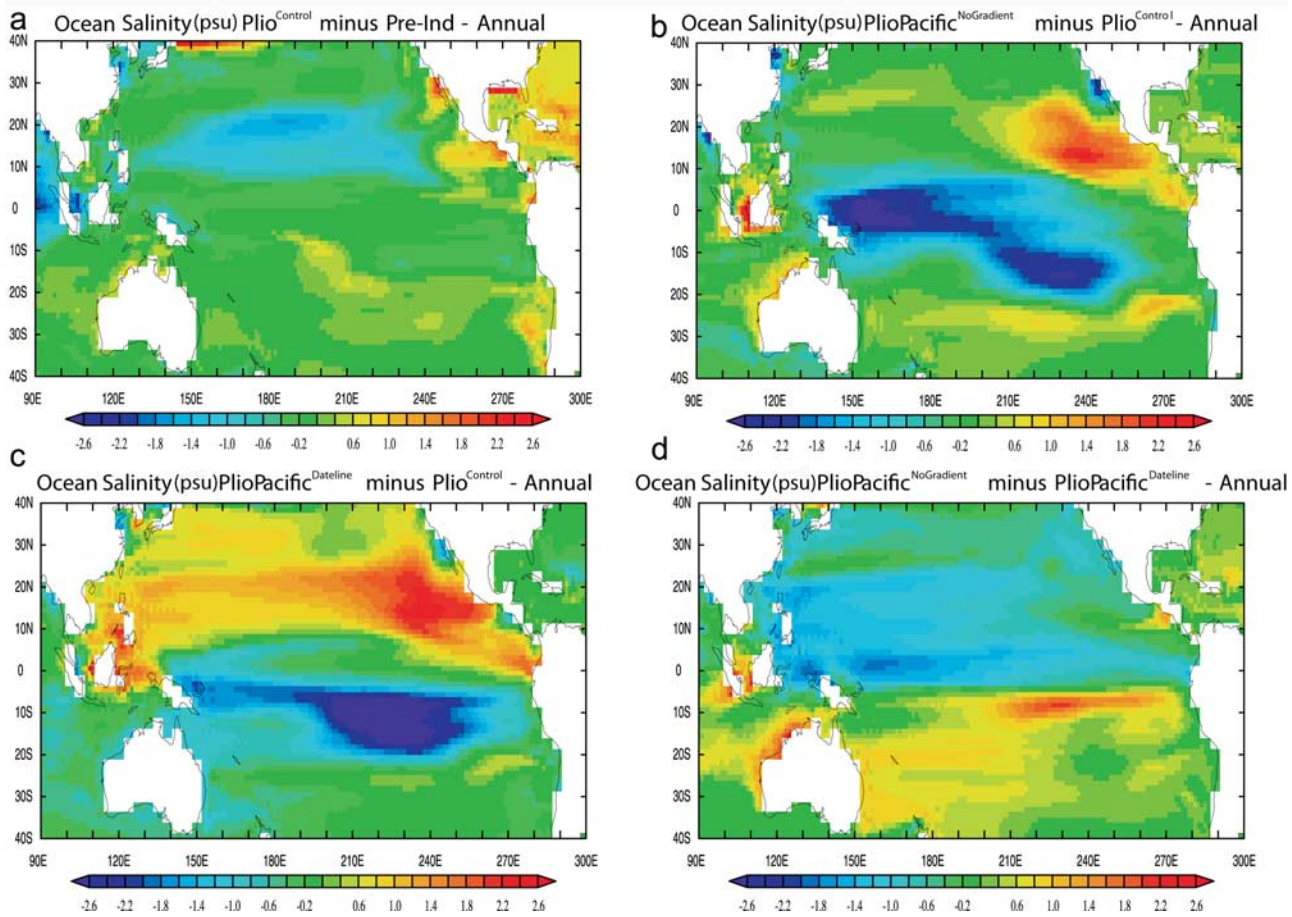

Figure 3. Differences in annual mean Pacific Ocean surface salinity (psu). (a) Plio^{Control} minus Pre-Ind. (b) PlioPacific^{NoGradient} minus Plio^{Control}. (c) PlioPacific^{Dateline} minus Plio^{Control}. (d) PlioPacific^{NoGradient} minus PlioPacific^{Dateline}.

the absence of an east-west SST gradient in experiments PlioPacific^{NoGradient}, PlioPacific^{Dateline} and PlioGlobal^{Dateline}, the surface trades in the equatorial Pacific region become weak. The Walker circulation collapses with upper level westerlies being replaced by easterlies at all levels. In experiments Pre-Ind and Plio^{Control} there is only one region of wind convergence over the tropical oceans marking the position of the ITCZ (Figure 5). In experiments PlioPacific^{NoGradient}, PlioPacific^{Dateline} and PlioGlobal^{Dateline}, in the absence of east-west SST gradient, there is a more clearly defined and broader region of surface wind convergence. A similar feature was identified in the *Barreiro et al.* [2005] study.

3.5. Tropical Pacific Cloud Cover (Percent)

[35] Altered tropical Pacific cloud cover, specifically a reduction in coverage of low-level stratus clouds, is predicted to be one of the principal effects of a permanent El Niño–like state [*Philander and Fedorov*, 2003]. Model predictions for the coverage (%) of low cloud in the Pacific for DJF and JJA are shown in Figure 6. The response of low cloud in experiment Plio^{Control} is mixed. However, low-cloud coverage is predicted to increase in the EEP by 1 to 20% during DJF and 1 to 15% during JJA. This pattern is reversed in sensitivity experiments PlioPacific^{NoGradient}, PlioPacific^{Dateline} and PlioGlobal^{Dateline} with low-cloud cover in the EEP being reduced by 1 to 15% during DJF and JJA compared to experiment Plio^{Control}.

3.6. Transmission of ENSO Signals to the High Latitudes

[36] A key feature of the surface temperature results from experiments PlioPacific^{NoGradient}, PlioPacific^{Dateline} and PlioGlobal^{Dateline} is that the high latitudes of the Northern and/or Southern Hemisphere cool in response to the warmer SSTs and altered SSTs gradients in the tropics. This cooling partly, or wholly, compensates for the tropical warming ensuring the global mean surface temperatures in these experiments remains similar to the Plio^{Control} simulation.

[37] The mechanisms and processes driving teleconnections associated with ENSO between the tropical Pacific and the poles are complex and only partially understood. *Hoskins and Karoly* [1981] were the first to demonstrate that an area of deep convection close to the equator can act as a generator of Rossby waves through the vorticity generated by diabatic heating. These Rossby wave trains travel poleward in both hemispheres and provide a means for the establishment of teleconnections between ENSO and the climates of the midlatitude areas [*Turner*, 2004; *Hoskins*

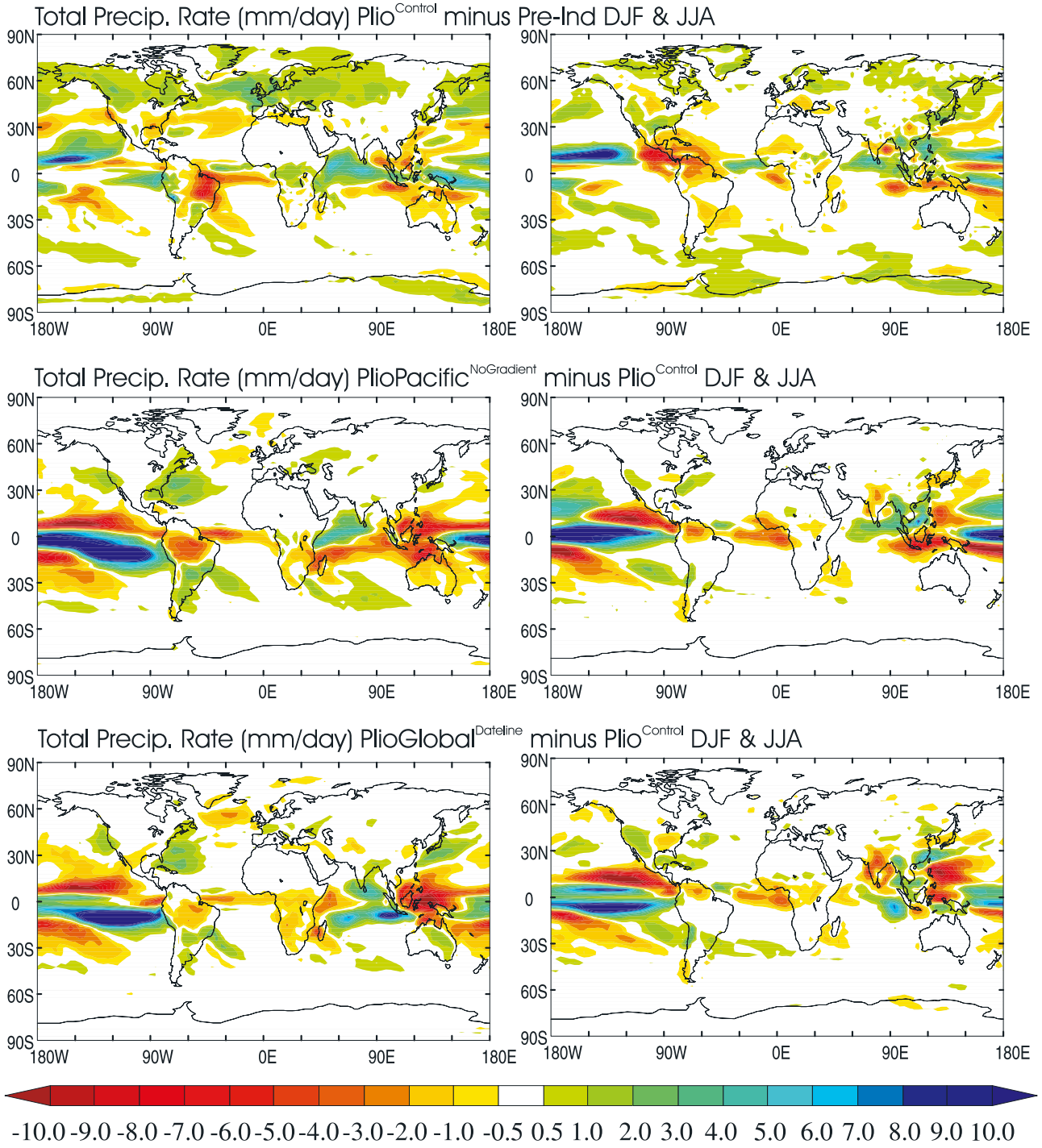

Figure 4. Results for total precipitation rate (mm d^{-1}) for (left) DJF and (right) JJA. (top) difference between experiments $Plio^{Control}$ and Pre-Ind. (middle) Difference between experiments $PlioPacific^{NoGradient}$ and $Plio^{Control}$. (bottom) Difference between $PlioGlobal^{Dateline}$ and $Plio^{Control}$.

and Karoly, 1981]. If such Rossby wave propagation occurs it is likely to manifest itself as a series of positive and negative atmospheric geopotential height anomalies moving away from the equator toward the poles [*Hoskins and Karoly*, 1981].

[38] *Held et al.* [1989] proposed that a tropically forced wave train could displace the downstream portion of the oceanic storm track so that small changes in tropical SSTs could have a large extra tropical response. *Rasmusson* [1991] and *Hoerling and Kumar* [1997] have demonstrated that there is a clear signal of ENSO warm events transmitted

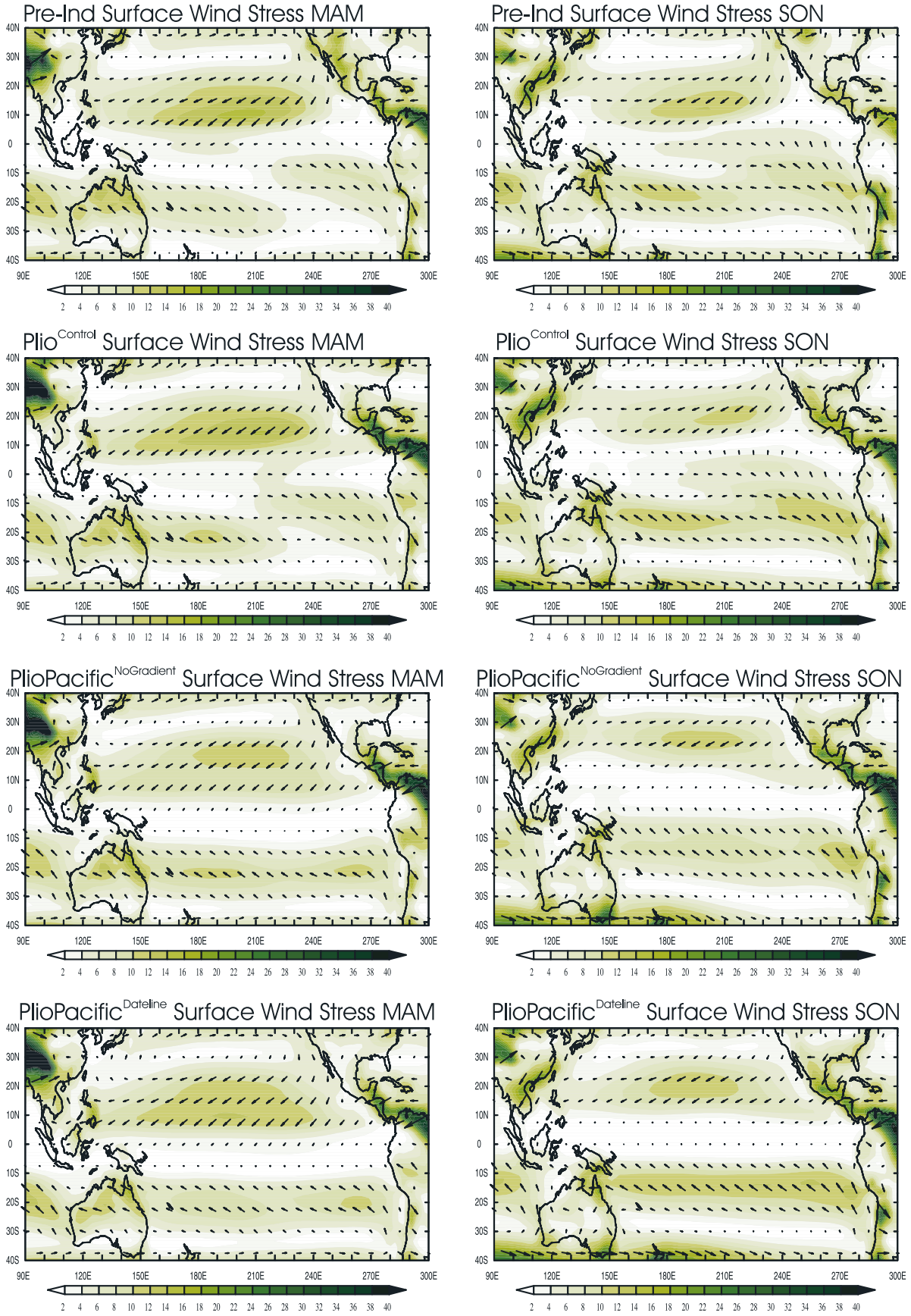
Pre-Ind Surface Wind Stress MAM
Pre-Ind Surface Wind Stress SON
Plio^Control Surface Wind Stress MAM
Plio^Control Surface Wind Stress SON
PlioPacific^NoGradient Surface Wind Stress MAM
PlioPacific^NoGradient Surface Wind Stress SON
PlioPacific^Dateline Surface Wind Stress MAM
PlioPacific^Dateline Surface Wind Stress SON
40N 30N 20N 10N 0 10S 20S 30S 40S
90E 120E 150E 180E 210E 240E 270E 300E
2 4 6 8 10 12 14 16 18 20 22 24 26 28 30 32 34 36 38 40

Figure 5

northward via Rossby wave trains known as the Pacific North American (PNA) pattern. The Southern Hemisphere equivalent to the PNA, the Pacific South American (PSA) pattern, affects the synoptic conditions across the southern part of South America and the Antarctic Peninsula [*Ruttlant and Fuenzalida*, 1991; *Harangozo*, 2000]. *Turner* [2004] argues that the most pronounced signals of ENSO in Antarctica are found over the southeast Pacific as a result of a climatological Rossby wave train that gives positive height anomalies over the Amundsen-Bellingshausen Sea during El Niño events and negative height anomalies during La Niña events [*Turner*, 2004].

[39] Given the similarities between the modeled responses in the Southern Hemisphere winter season 500 hPa height field in experiments PlioPacific^{NoGradient}, PlioPacific^{Dateline} and PlioGlobal^{Dateline} and the studies of *Hoskins and Karoly* [1981] and *Turner* [2004], who used NCEP-NCAR reanalysis data of the last eight El Niño events, we conclude that the altered SST patterns in these experiments initiated a Rossby wave train from the tropics to the South Pacific (Figure 7). The PSA pattern of upper air height and surface pressure anomalies results in higher pressures (greater ridging or blocking) west of the Antarctic Peninsula. The net result of positive mean sea level pressure anomalies over the Bellingshausen/Scotia Sea regions is a circulation pattern that gives greater southerly component to the winds over the Peninsula resulting in negative temperature anomalies (Figure 1). Reduced SSTs in this region are then propagated (and in certain regions amplified) around the rest of Antarctica via feedbacks associated with the Antarctic Circumpolar Current (ACC) and the atmosphere/sea-ice interactions. This interpretation is supported by the work of *White and Peterson* [1996] suggesting that ocean circulation could indeed play a role in the transmission of ENSO signals to the southern high latitudes via the Antarctic Circumpolar Wave (ACW). Additionally, *Cai and Baines* [2001] suggest that the atmospheric wind stress and heat flux anomalies induced by the PSA wave train caused SST changes of around 1°C over large areas of the South Pacific, which were then advected eastward by the ACC. They suggest that the principle component of the ACW is initiated by atmospheric teleconnections via the PSA, propagated by the ACC and maintained by air-sea interactions [*Cai and Baines*, 2001].

[40] T. Lachlan-Cope and W. Connolley (Teleconnections between the tropical Pacific and the Amundsen-Bellingshausen Sea—The role of the El Niño/Southern Oscillation, unpublished manuscript, 2006, hereinafter referred to as Lachlan-Cope and Connolley, unpublished manuscript, 2006) concur that tropical Pacific–high southern latitude teleconnections are caused by Rossby wave dynamics, but they also propose that they are sensitive to the exact pattern of SST anomalies forcing anomalous ascent. This may help to explain the differences observed in the high-latitude response between experiment PlioPacific^{NoGradient} and experiments PlioPacific^{Dateline} and PlioGlobal^{Dateline}. In the experiments of Lachlan-Cope and Connolley (unpublished manuscript, 2006) differences are observed between the high-latitude responses to El Niño with apparently similar tropical forcings that make accurate prediction of the high-latitude response to tropical change difficult. Their ensemble GCM runs demonstrate that variations due to the natural variation of the zonal flow in the Southern Hemisphere can swamp the signal resulting from changes in the Rossby wave source region.

[41] Experiments PlioPacific^{Dateline} and PlioGlobal^{Dateline} exhibit cooling in the high latitudes of Northern Hemisphere as well as around Antarctica (Figure 1). In the Northern Hemisphere positive height anomalies, relative to experiment Plio^{Control}, of up to 120 m in the DJF 500 hPa field are noted in both experiments (Figure 7). These are centered on the Canadian North West Territories. A negative height anomaly of up to 80 m is also predicted over the NW Pacific Ocean in both experiments and over the Baltic and Russian Arctic (~80 m) in experiment PlioGlobal^{Dateline} (Figure 7). Associated with this are large changes in the DJF mean sea level pressure field in the high-latitude low-pressure centers (e.g., Icelandic Low) and smaller, but still significant changes to subtropical high-pressure centers (e.g., Azores High). Mean sea level pressure increases at the high latitudes and decreases in the subtropics relative to experiment Plio^{Control} (Figure 8). The net affect of this change is to reduce the strength of DJF westerly wind stress in the Northern Hemisphere, a change that may, at least in part, explain the cooling in the Northern Hemisphere (relative to experiment Plio^{Control}) high latitudes. Reduced winter storm strength could weaken the net amount of heat transported into the Arctic. This effect may then be amplified by air-sea ice interactions in a similar manner as occurs around Antarctica.

4. Discussion

4.1. ENSO in a Fully Coupled mid-Pliocene Ocean-Atmosphere GCM

[42] In statistics and signal processing, the method of empirical orthogonal function (EOF) analysis is a decomposition of a signal or data set in terms of orthogonal basis functions that are determined from the data. It is the same as performing a principal components analysis on the data, except that the EOF method finds both time series and spatial patterns. Figure 9a shows two EOF analyses for experiment Plio^{Control} and Pre-Ind (land areas masked out) equatorial Pacific SSTs. For both experiments a clear pattern of ENSO is distinguished in the first EOF accounting for 22.5% and 18.47%, respectively, of the variance in the model results. This represents a 22% increase in equatorial Pacific SST variability in the mid-Pliocene scenario although it is unclear if this change is statistically significant and therefore physically meaningful. We have also examined the interannual variability of surface air temperatures in both the Pre-Ind and Plio^{Control} experiments for El Niño region 3.4 (Figure 9b). The results indicate a greater degree

Figure 5. Surface wind stress results with wind stress directions (N m^{-2}) for MAM and SON for experiments Pre-Ind, Plio^{Control}, PlioPacific^{NoGradient} and PlioPacific^{Dateline}.

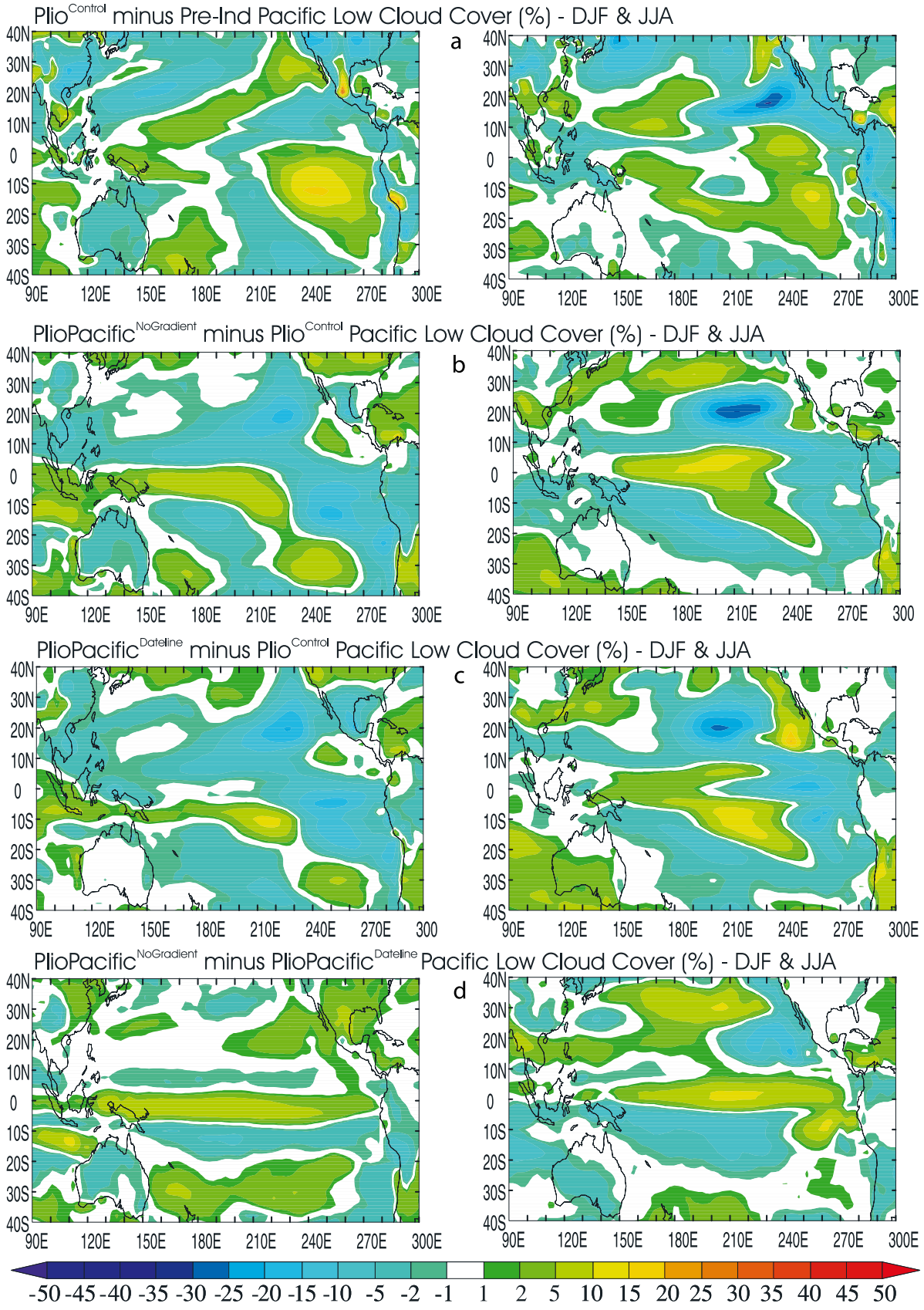
Plio^Control minus Pre-Ind Pacific Low Cloud Cover (%) - DJF & JJA
a
PlioPacific^NoGradient minus Plio^Control Pacific Low Cloud Cover (%) - DJF & JJA
b
PlioPacific^Dateline minus Plio^Control Pacific Low Cloud Cover (%) - DJF & JJA
c
PlioPacific^NoGradient minus PlioPacific^Dateline Pacific Low Cloud Cover (%) - DJF & JJA
d
40N 30N 20N 10N 0 10S 20S 30S 40S
90E 120E 150E 180E 210E 240E 270E 300E
-50 -45 -40 -35 -30 -25 -20 -15 -10 -5 -2 -1 1 2 5 10 15 20 25 30 35 40 45 50

Figure 6

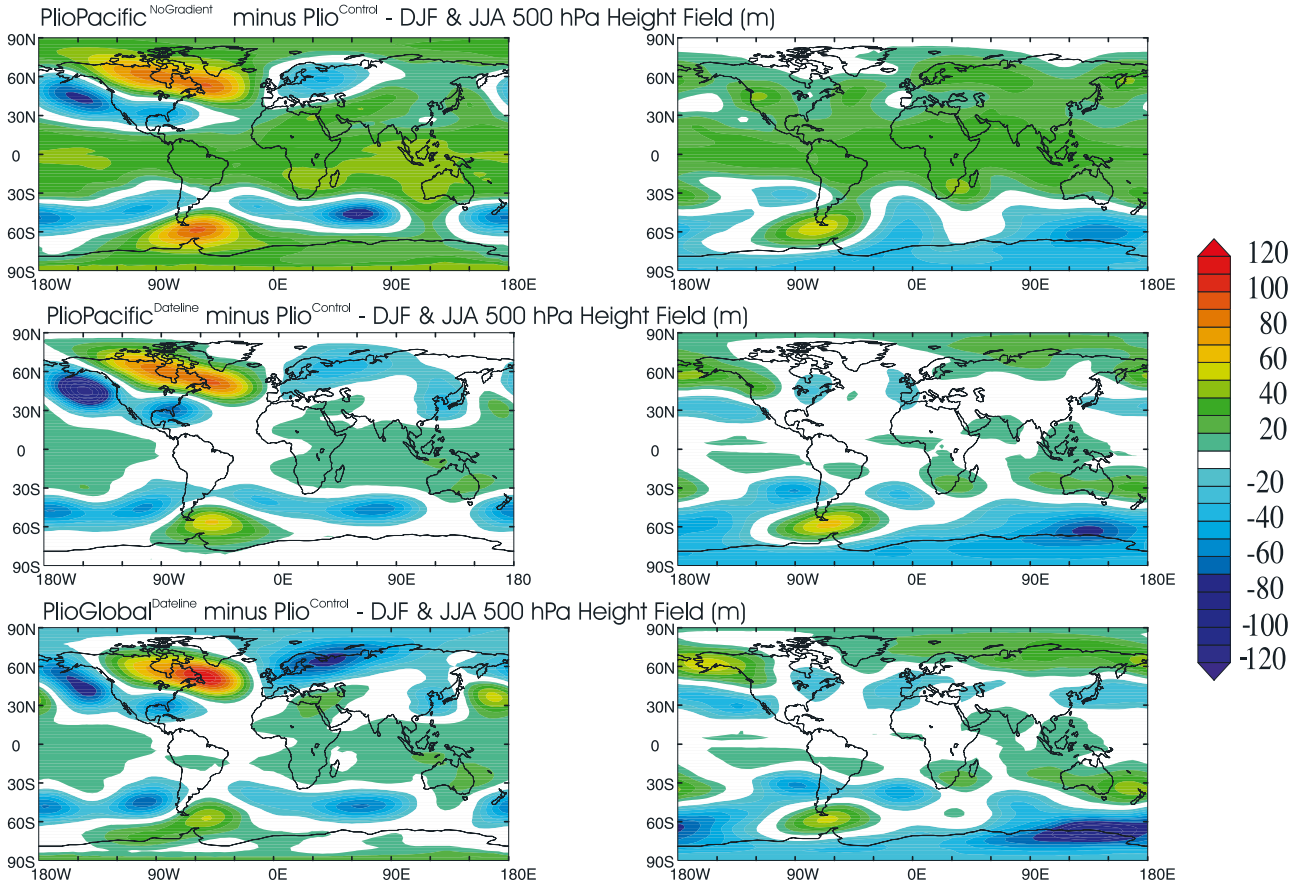

Figure 7. The 500 hPa height field results (m) for (left) DJF and (right) JJA. (top) Difference between experiments Plio^{NoGradient} and Plio^{Control}. (middle) Difference between experiments PlioPacific^{Dateline} and Plio^{Control}. (bottom) Difference between experiments PlioGlobal^{Dateline} and Plio^{Control}.

of surface air temperature variability (20% increase) in experiment Plio^{Control}.

[43] In a further effort to examine differences in the interannual variability of surface air temperatures between the Pre-Ind and the Plio^{Control} simulation we have examined one hundred years of modeled interannual variability of DJF surface air temperatures from geographical location corresponding to ODP Sites 806, 847 and 851. These represent the three principal sites used to derive the paleoceanographic data suggesting permanent El Niño–like or La Niña–like conditions for the Pliocene (Figure 10). Surface air temperatures for the Plio^{Control} experiment are, as one would expect, higher than the preindustrial because of a greater concentration of CO_2 in the atmosphere. However, analyses of the standard deviations of the data indicate that there is either the same or more variance in surface air temperatures in the Plio^{Control} experiment for ODP Sites 847 and 851 (EEP) and substantially greater variance at site 806 (WEP).

[44] These results clearly demonstrate ENSO events in experiments Plio^{Control} and Pre-Ind, and that these events account for the same, or more, of the SST and surface air temperature variability in experiment Plio^{Control} than they do in experiment Pre-Ind. This provides strong evidence to support our assertion that ENSO is at least as well expressed in the mid-Pliocene case, perhaps stronger in the WEP, as it is in the preindustrial experiment.

4.2. Data/Model Comparison

[45] Is it possible to reconcile the results of the HadCM3 GCM with paleoceanographic data? Both a permanent El Niño– and La Niña–like condition has been interpreted from Pacific Ocean Mg/Ca, $\delta^{18}O$ and alkenone-based SST estimates [e.g., *Haywood et al.*, 2005; *Ravelo et al.*, 2004; *Wara et al.*, 2005; *Rickaby and Halloran*, 2005]. Given the temporal resolution of the data, which is at best 1 sample per 10,000 years, it is clear that none of the records are capable of proving the existence of either a permanent El Niño– or La Niña–like state during the Pliocene since

Figure 6. Low cloud results (%) for (left) DJF and (right) JJA over the Pacific. (a) Difference between experiments Plio^{Control} and Pre-Ind. (b) Difference between experiments PlioPacific^{NoGradient} and Plio^{Control}. (c) Difference between PlioPacific^{Dateline} and Plio^{Control}. (d) Difference between PlioPacific^{NoGradient} and PlioPacific^{Dateline}.

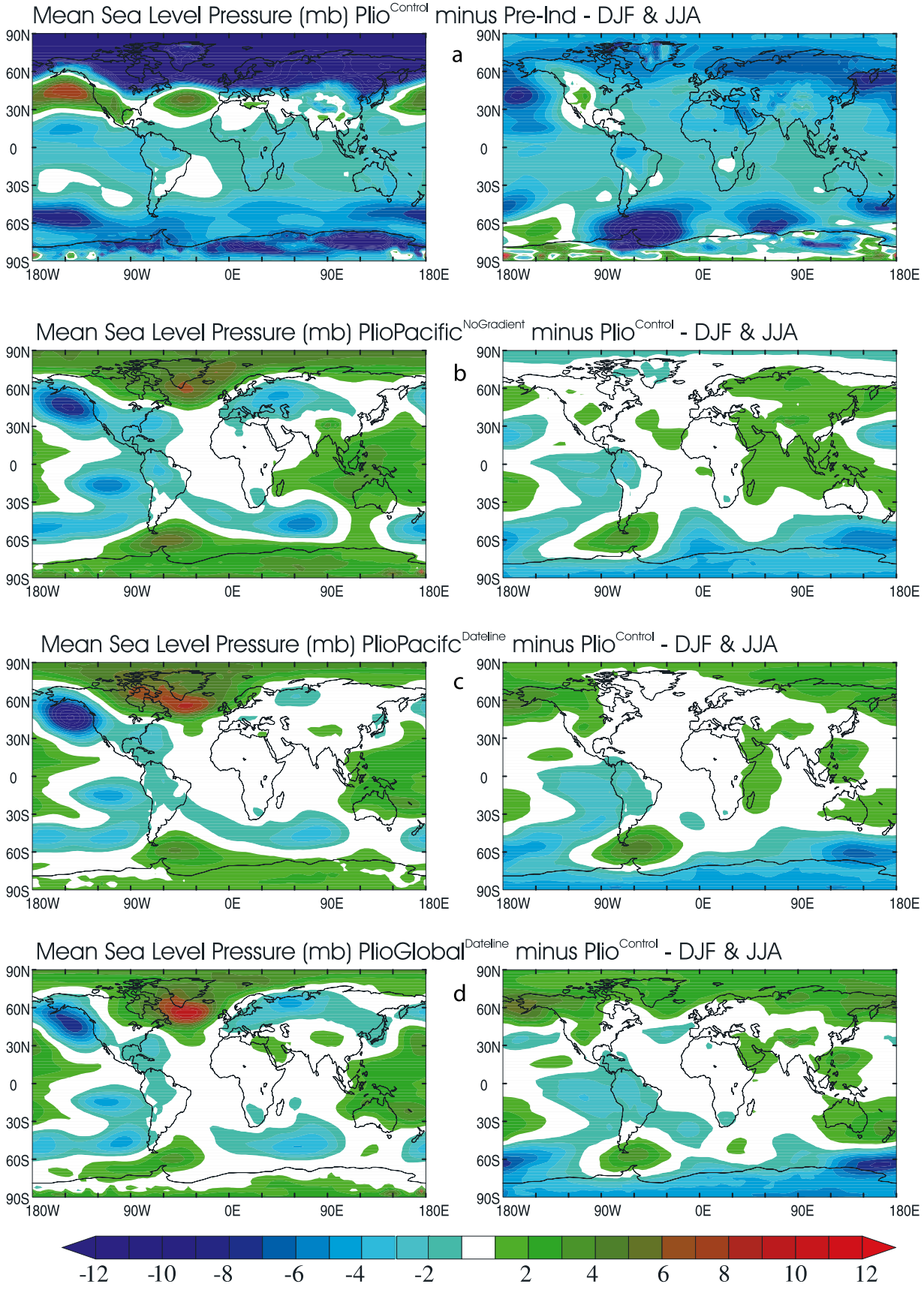
Mean Sea Level Pressure (mb) Plio^Control minus Pre-Ind - DJF & JJA
a
Mean Sea Level Pressure (mb) PlioPacific^NoGradient minus Plio^Control - DJF & JJA
b
Mean Sea Level Pressure (mb) PlioPacifc^Dateline minus Plio^Control - DJF & JJA
c
Mean Sea Level Pressure (mb) PlioGlobal^Dateline minus Plio^Control - DJF & JJA
d
90N
60N
30N
0
30S
60S
90S
180W
90W
0E
90E
180E
-12 -10 -8 -6 -4 -2 2 4 6 8 10 12

Figure 8

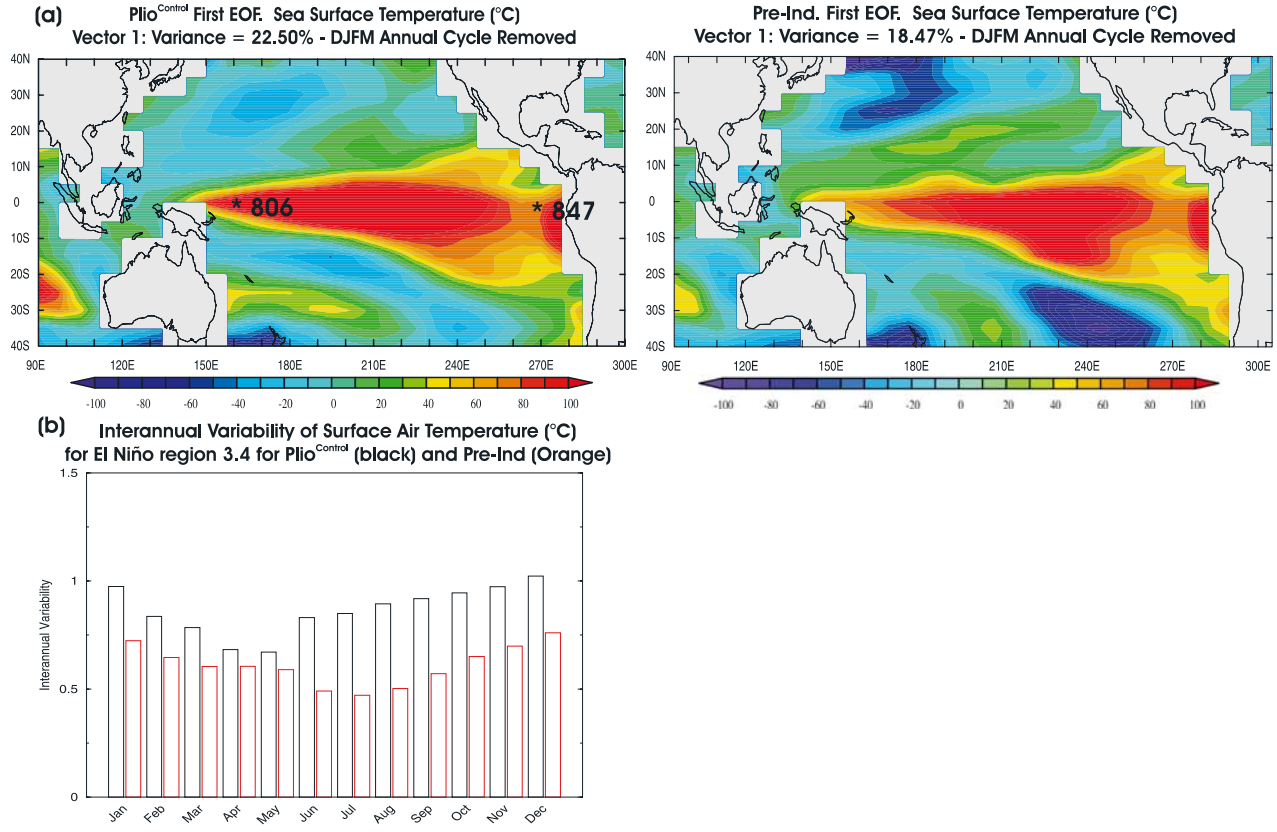

Figure 9. (a) Leading (first) EOF for SSTs (°C) in the tropical Pacific (land areas masked out and annual cycle removed) for experiments (left) Plio^{Control} and (right) Pre-Ind. (b) Interannual variability of surface air temperatures (°C) for El Niño region 3.4 for experiment Plio^{Control} and Pre-Ind.

ENSO events occur over decadal to subdecadal timescales. Ideally, an approach capable of documenting SST variability at an annual or even subannual resolution would be used (for example, stable isotope or Mg/Ca analysis of annual growth layers of mollusc shells or corals [cf. *Roulier and Quinn*, 1995]). What the data sets do provide are snap shots of the mean state of tropical Pacific SSTs at specific geographical locations during the Pliocene.

[46] *Wara et al.* [2005] have characterized the change in the mean state as representing warmer SSTs in the EEP (~2°C) and cooler SSTs in the WEP (~2°C). Relative to today this reduces the SST gradient across the Pacific during the Pliocene which they argue is indicative of a permanent El Niño–like condition. Our modeling results concur with their reconstructed change in the mean state of EEP SSTs. However, WEP SSTs in our model also warm.

[47] A controversy has arisen over the reliability of Pliocene Mg/Ca–derived Pacific SST records [*Kerr*, 2005] because of the conflicting interpretations of mean state changes to equatorial Pacific SSTs provided by the *Wara et al.* [2005] and *Rickaby and Halloran* [2005] data sets. Although they use the same core material and proxy approach, *Rickaby and Halloran* [2005] challenge the permanent El Niño scenario of *Wara et al.* [2005], claiming "SSTs in the WEP warm pool remain relatively stable and consistently warmer than the EEP during the Pliocene," which they infer as representing a permanent La Niña–like state. The two studies reproduce Mg/Ca values well within the expectations of interlaboratory analysis (±8% [*Rosenthal et al.*, 2004]) (Figure 11a) for the majority of the record. Different Mg/Ca–SST calibrations were applied in the two studies such that SST estimates derived by *Rickaby and Halloran* [2005] are, on average, 2.5°C cooler than those of *Wara et al.* [2005] (Figure 11c), however the relative offset between SST at the two core sites is independent of calibration choice (Figure 11b) and this control on reconstructed SST should not influence the interpretation of climate state. Rather, *Rickaby and Halloran* [2005] draw their La Niña–like state conclusion from two data points that are significantly removed from the high-resolution data

Figure 8. Mean sea level pressure results (mbar) for (left) DJF and (right) JJA. (a) Difference between experiments Plio^{Control} and Pre-Ind. (b) Difference between experiments PlioPacific^{NoGradient} and Plio^{Control}. (c) Difference between PlioPacific^{Dateline} and Plio^{Control}. (d) Difference between PlioGlobal^{Dateline} and Plio^{Control}.

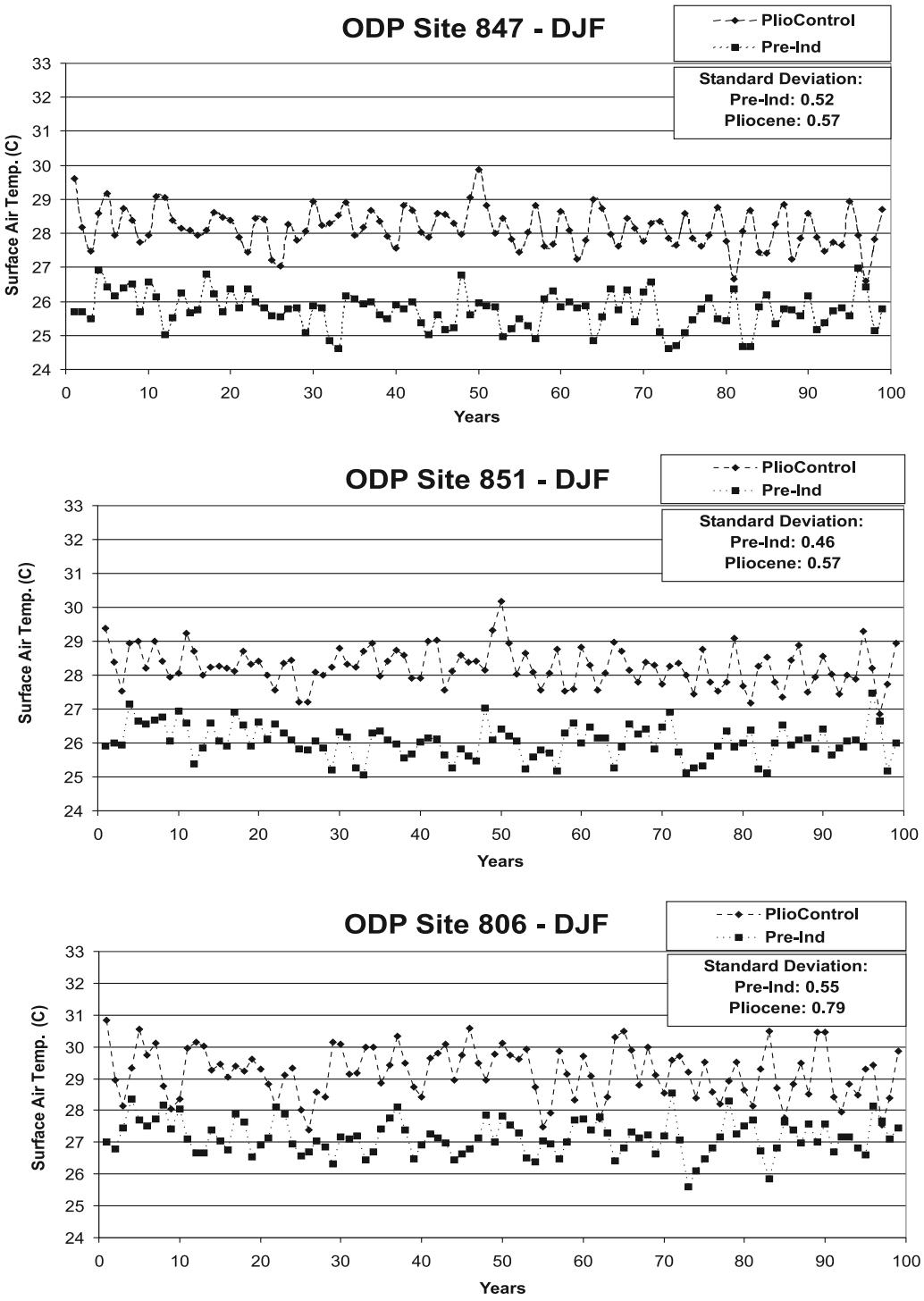

Figure 10. Time series of model-predicted DJF surface air temperatures (°C) for experiments $Plio^{Control}$ and Pre-Ind at coordinates corresponding to the positions of Ocean Drilling Program (ODP) Sites 847 (EEP), 851 (EEP), and 806 (WEP). Note standard deviation for experiment $Plio^{Control}$ exceeds the standard deviation for experiment Pre-Ind at each site.

set of *Wara et al.* [2005], suggesting >5°C cooler SSTs in the EEP and an equatorial gradient similar to, if not greater, than today within the interval 6 to 4 Ma. Although the cleaning method of *Rickaby and Halloran* [2005] incorporating a reductive step is claimed to produce a more accurate SST record, the scarcity of data is a concern and further analyses, preferably corroborated by a multiproxy approach, are necessary to validate this interpretation.

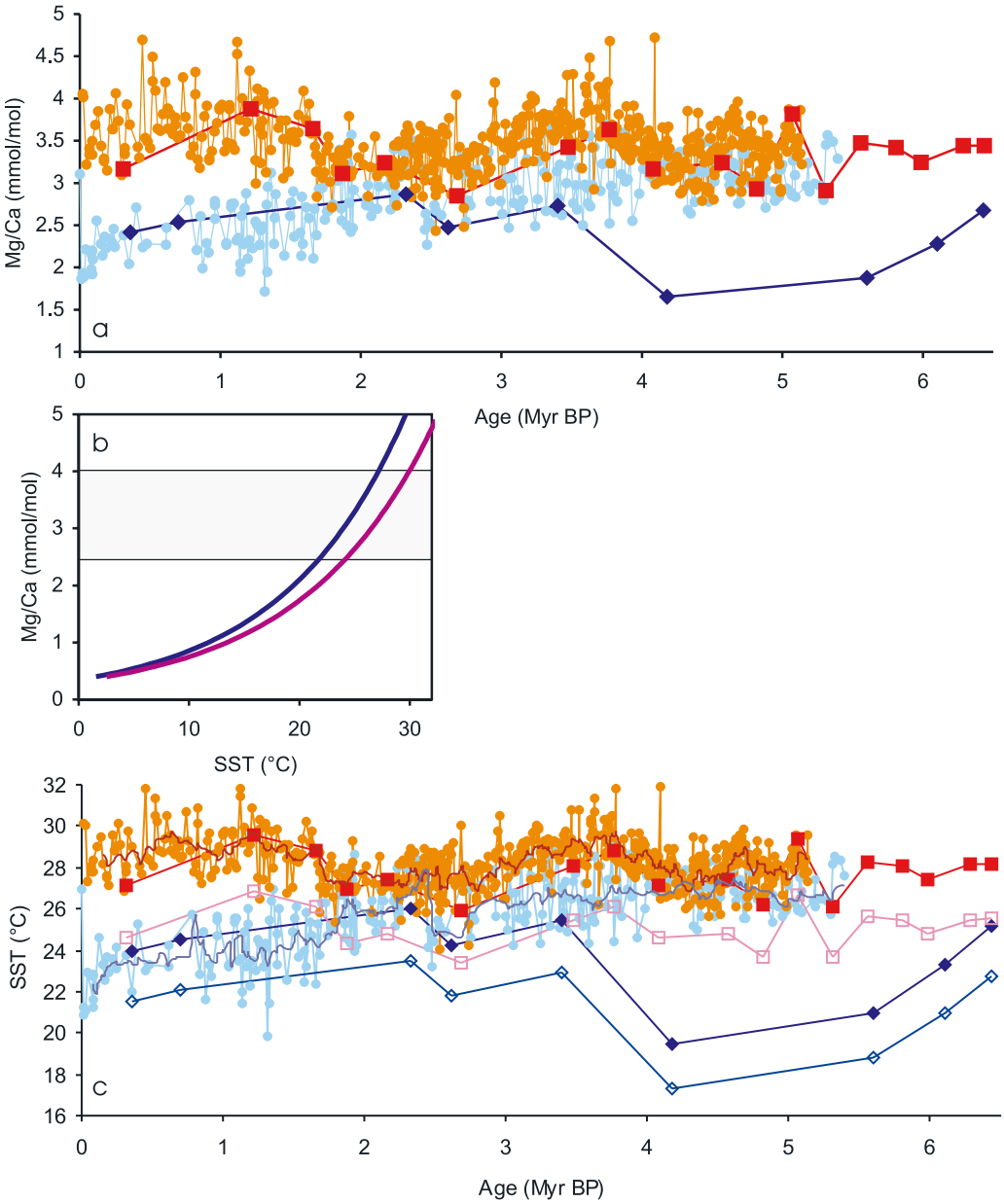

Figure 11. Comparison of equatorial Pacific Mg/Ca–based SST records. (a) Mg/Ca measurements from ODP Site 806 in the WEP (orange-red) and ODP Site 847 in the EEP (blue). *Wara et al.* [2005] data points are indicated by circles. *Rickaby and Halloran* [2005] data points are indicated by squares/diamonds. (b) Mg/Ca–SST calibration of *Dekens et al.* [2002], used by *Wara et al.* [2005], in pink and Mg/Ca–SST calibration of *Anand et al.* [2003], used by *Rickaby and Halloran* [2005], in blue. Grey bar highlights average Mg/Ca values presented in Figure 11a. (c) SST records for both data sets using the Mg/Ca–SST calibration of *Dekens et al.* [2002]. Published records of *Rickaby and Halloran* [2005] using the *Anand et al.* [2003] Mg/Ca–SST calibration are indicated by open squares/diamonds.

[48] It is well known that the δ^{18}O of planktonic foraminifera is not simply related to ocean temperature. Figure 12 shows diagnostic model outputs for the change in the δ^{18}O of seawater (δ^{18}Osw) based on the climate model's predicted P – E budget. This demonstrates that relatively small variations in SSTs can generate large changes in the predicted δ^{18}Osw in the equatorial Pacific. Predicted differences in the δ^{18}Osw between the Plio$^{\text{Control}}$ experiment and experiments PlioPacific$^{\text{NoGradient}}$ and PlioPacific$^{\text{Dateline}}$ are up to −0.5‰ at ODP Site 806 and +0.2‰ at ODP Site 847, which is significant considering that the maximum difference in δ^{18}O values recorded by *G. sacculifer* between ODP Site 806 and 847 during the last 5.5 million years, in the study of *Wara et al.* [2005], is ∼0.8‰. Therefore our results

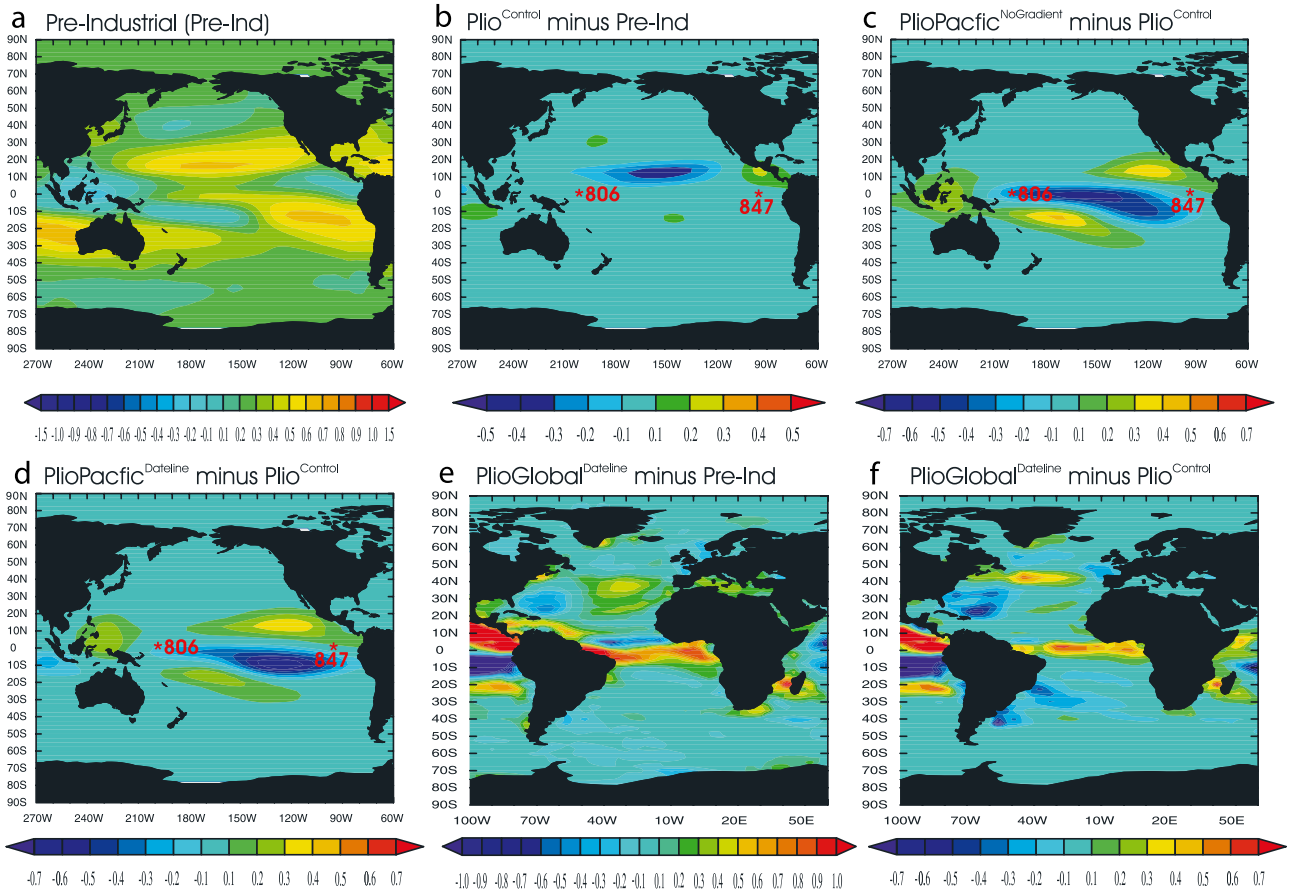

Figure 12. Diagnostic predictions of δ^{18}Osw (‰) based on model-predicted precipitation minus evaporation values (see section 2.4 for more details). (a) Prediction of Pacific Ocean δ^{18}Osw for experiment Pre-Ind (using Pacific calibration). (b) Prediction of Pacific Ocean δ^{18}Osw for experiment Plio$^{\text{Control}}$ (using Pacific calibration, locations of ODP Sites 806 and 847 marked). (c) Prediction of Pacific Ocean δ^{18}Osw for experiment PlioPacific$^{\text{NoGradient}}$ minus Plio$^{\text{Control}}$ (using Pacific calibration, locations of ODP Sites 806 and 847 marked). (d) Prediction of Pacific Ocean δ^{18}Osw for experiment PlioPacific$^{\text{Dateline}}$ minus Plio$^{\text{Control}}$ (using Pacific calibration, locations of ODP Sites 806 and 847 marked). (e) Prediction of Atlantic Ocean δ^{18}Osw for experiment PlioGlobal$^{\text{Dateline}}$ minus Pre-Ind (using Atlantic calibration). (f) Prediction of Atlantic Ocean δ^{18}Osw for experiment PlioGlobal$^{\text{Dateline}}$ minus Plio$^{\text{Control}}$ (using Atlantic calibration).

suggest that a significant proportion of the reconstructed change in δ^{18}O values might relate to salinity change rather than SST, further complicating how the data are interpreted.

[49] In a related study of ENSO behavior during the Eocene by *Huber and Caballero* [2003], no evidence was found for a shift toward a permanent El Niño–like condition. *Huber and Caballero* [2003] compared a coupled ocean-atmosphere climate model simulation with annually resolved variability records preserved in lake sediments. The simulations show Pacific deep ocean and high-latitude surface warming of ~10°C but little change in the tropical thermocline structure, atmosphere-ocean dynamics, and ENSO, in agreement with proxies. In this study atmospheric CO_2 levels were prescribed at a level substantially higher than Pliocene values, yet this was insufficient to generate changes in the thermocline necessary to produce a permanent El Niño–like state. If such a state did not occur during the warmth of the Eocene we are left to wonder why it should occur during the relatively cooler mid-Pliocene.

[50] Similarly, *Munoz et al.* [2002] studied an exceptional sequence of 1745 varves in the Villarroya Pliocene Basin (Spain). Time series of light, dark, and the sum of both layers, were performed. Periodicities of ~12, 6–7 and 2–3 years were obtained. *Munoz et al.* [2002] argue that the origin of these periodicities could relate to natural phenomena like sunspot cycles, ENSO, NAO or the Quasi-biennial Oscillation, as these phenomena are capable of modulating the climate in these frequency bands. If so this might provide independent sedimentological evidence for ENSO events during the Pliocene that support our modeling results.

[51] *Fedorov et al.* [2006] discuss the initial results from our mid-Pliocene fully coupled ocean atmosphere simulation, published by *Haywood and Valdes* [2004]. *Fedorov et*

al. [2006] argue that our model-predicted SSTs are inconsistent with 'observations' (by which they mean proxy reconstructions) over the last 10 million years showing that SSTs in the WEP never exceeded 30°C. This conclusion is based on the consideration of difference fields presented by *Haywood and Valdes* [2004] and not on the absolute SST's predicted for the mid-Pliocene. When absolute SSTs in the WEP are compared to proxy data we find no discrepancy between the data and model. In experiment $Plio^{Control}$ annual mean temperatures at the ocean surface at the geographical location corresponding to ODP Site 806 (WEP) are 29.77°C. In experiment Pre-Ind ocean surface temperatures are 27.98°C. At a geographical location corresponding to the position of ODP site 847 (EEP) $Plio^{Control}$ annual mean temperatures at the ocean surface are 27.85°C. In experiment Pre-Ind ocean surface temperatures are 26.14°C. At both ODP Sites 806 and 847, SSTs are warmer in the mid-Pliocene scenario but WEP SST's do not exceed 30°C. The annual mean SST gradient between ODP sites 806 and 847 is 1.92°C in experiment $Plio^{Control}$. The model-predicted gradient in tropical Pacific SSTs in experiment $Plio^{Control}$ concurs with proxy reconstructions presented by *Wara et al.* [2005, p. 758] in which it is stated that "during the warm early Pliocene the average west-to-east sea surface temperature difference across the equatorial Pacific was only 1.5°C (±0.9°C), much like it is during a modern El Niño event." Therefore our model predicts a west-to-east SST gradient in agreement with proxy reconstructions that could be used to support the premise of a permanent El Niño–like state during the mid-Pliocene yet ENSO variability is clearly displayed by our model (see Figures 9 and 10).

4.3. Mid-Pliocene Warmth and the Initiation of Northern Hemisphere Glaciation

[52] It has been proposed by *Philander and Fedorov* [2003] and *Barreiro et al.* [2005] that changes in the zonal gradient of SST across the tropics might have played an important role in maintaining pre-Pleistocene warm periods, and also contributed to the onset of Northern Hemisphere glaciation (NHG). This is part of a substantial body of research that underlines the importance of tropical atmospheric and oceanic processes on global climate [e.g., *Latif et al.*, 2000; *Thorpe et al.*, 2001].

[53] To date the modeling studies that have highlighted the link between SST gradients in the tropics (permanent El Niño–like condition) and global temperatures of the mid-Pliocene have been conducted using atmosphere-only GCMs, running with present-day boundary conditions and fixed SSTs [*Philander and Fedorov*, 2003; *Barreiro et al.*, 2005]. Our approach has been different as we have assessed whether or not a coupled ocean-atmosphere GCM, initialized with a comprehensive set of mid-Pliocene boundary conditions, is (1) capable of reproducing a permanent El Niño–like or La Niña–like state, and (2) what the impact on the coupled ocean-atmosphere system is when such a state is specified as a prescribed boundary condition in the model. Our results do not support the notion of a permanent El Niño–like state (or La Niña) during the mid-Pliocene. Nor do they indicate that such a condition, if prescribed, significantly changes global mean temperatures, since part or all of the tropical SST change is offset by opposite changes at high latitudes. Therefore the direct effect of a transition out of a permanent El Niño–like state during the Late Pliocene will be a small (maximum 0.6°C) cooling of global climate. Moreover, the substantial high-latitude warming associated with this transition (as shown in experiments $PlioPacific^{Dateline}$ and $PlioGlobal^{Dateline}$) could inhibit the expansion of ice in the Northern Hemisphere, although we recognize that most cooling occurs in the Northern Hemisphere winter season which is not the most important season for ice sheet initiation. The resulting snow accumulation predicted by the model over Greenland shows either very little change (experiments $PlioPacific^{NoGradient}$ and $PlioGlobal^{Dateline}$), or a tendency to increase accumulation rates with a prescribed permanent El Niño–like state (experiment $PlioPacific^{Dateline}$), which is inconsistent with the premise that the transition out of a permanent El Niño–like state was a major driver of NHG.

[54] Given the differences in experimental design between our modeling studies and those of *Philander and Fedorov* [2003] and *Barreiro et al.* [2005], and the differences in the relative complexity of the model set up (atmosphere-only GCM running with preindustrial boundary conditions and prescribed SSTs versus a fully coupled mid-Pliocene ocean-atmosphere GCM with predicted SSTs) it is not altogether surprising that our conclusions differ from previous work. As well as the set up and configuration of models used, the models differ substantially in terms of their physical parameterizations leading to variations in the way different models simulate ENSO and other processes such as cloud-radiative feedbacks.

[55] However, even with these limitations, when our results are viewed together with the uncertainties we have highlighted in the paleoceanographic data, there is sufficient cause to reconsider a number of assumptions that have been made concerning the role of El Niño (or La Niña) in Pliocene climate change and the onset of NHG.

4.4. Further Work

[56] This work has demonstrated that when a comprehensive set of mid-Pliocene boundary conditions are used to initialize the HadCM3 GCM ENSO events are clearly expressed by the model. Predicted mean SST increases in the EEP, in agreement with paleoceanographic data from ODP Sites 847 and 851. The depth of the thermocline across the equatorial Pacific is similar to the preindustrial being relatively deep in the WEP and at or near the surface in the EEP. Whilst the model results support a mean warming in EEP SSTs they are incapable of reproducing either a permanent El Niño or La Niña–like condition.

[57] Our experiments are sophisticated but they only provide a snap shot of the Pliocene (mid-Pliocene), as they do not encompass all of the boundary condition changes that are possible for the epoch. Further simulations designed to examine the importance of an open Panama gateway and altered Indonesian throughflow on Pliocene Pacific SST gradients, and for the behavior of Pliocene ENSO, are required to test our results and will be the subject of a future study. Furthermore, the use of an oxygen isotope

enabled GCM is required to more robustly forward model the $\delta^{18}O$ composition of Pliocene seawater.

5. Concluding Remarks

[58] The approach in this study was to use a coupled ocean-atmosphere GCM to explore the notion that the mid-Pliocene may have been characterized by permanent El Niño–like [*Wara et al.*, 2005] or La Niña–like [*Rickaby and Halloran*, 2005] condition. We have also examined the hypothesis that a permanent El Niño–like state may have contributed to the warmth of the Pliocene and subsequently played a role on the initiation of Northern Hemisphere glaciation (NHG) [*Philander and Fedorov*, 2003; *Barreiro et al.*, 2005]. Five model simulations are presented and include one preindustrial run, a Pliocene control simulation (to investigate if a permanent El Niño–like or La Niña–like state is predicted by the model), and three sensitivity experiments in which the sea surface temperature (SST) gradient across the Pacific and other ocean basins is altered. The sensitivity experiments were designed to investigate what the impact of a permanent El Niño–like state would be on the coupled ocean-atmosphere system and therefore, indirectly, what role it played in NHG.

[59] SSTs in the eastern equatorial Pacific increase in agreement with proxy data. However, ENSO events are clearly expressed in our control mid-Pliocene simulation and therefore are not compatible with the notion that the mid-Pliocene was characterized by either a permanent El Niño–like or La Niña–like condition.

[60] Sensitivity tests indicate that removing the gradient of SSTs across the Pacific does lead to reduced low-cloud cover, lower surface albedo values. Regional surface temperature warming can be substantial (e.g., up to 8°C over North America). However, high-latitude cooling in part, or wholly, compensates for this warming so that global annual mean temperatures remain virtually unchanged. On the basis of these modeling results it is unlikely that a permanent El Niño–like condition, if it existed, contributed significantly to global mid-Pliocene warmth and, therefore it is likely that the termination of this state had only a minor influence on NHG.

[61] **Acknowledgments.** The Natural Environment Research Council is acknowledged for supporting this work through the provision of High Performance Computing. This paper is published as part of the British Antarctic Survey's GEACEP programme, which investigates climate change over geological timescales. We thank the Harry Dowsett and the PRISM Group for use of their materials and Ana Christina Ravelo, Petra Dekens, and Ros Rickaby for thought-provoking discussions on Pliocene paleoceanographic data.

References

Achutarao, K., K. R. Sperber, and CMIP modelling Groups (2002), Simulation of El Niño Southern Oscillation: Results from the coupled model intercomparison project, *Clim. Dyn.*, *19*, 191–209.

Anand, P., H. Elderfield, and M. H. Conte (2003), Calibration of Mg/Ca thermometry in planktonic foraminifera from a sediment trap time series, *Paleoceanography*, *18*(2), 1050, doi:10.1029/2002PA000846.

Barreiro, M., G. Philander, R. Pacanowski, and A. Fedorov (2005), Simulations of warm tropical conditions with application to middle Pliocene atmospheres, *Clim. Dyn.*, doi:10.1007/s00382-005-0086-4.

Berggren, W. A., D. V. Kent, C. C. Swisher, and M. P. Aubry (1995), A revised Cenozoic geochronology and chronostratigraphy, in *Geochronology, Time Scales and Global Stratigraphic Correlation*, Tulsa, edited by W. A. Berggren et al., *Spec. Publ. Soc. SEPM Sediment. Geol.*, *54*, 129–212.

Bigg, G. R., and E. J. Rohling (2000), An oxygen isotope data set for marine waters, *J. Geophys. Res.*, *105*, 8527–8535.

Brown, J., M. Collins, and A. Tudhope (2006), Coupled model simulations of mid-Holocene ENSO and comparisons with coral oxygen isotope records, *Adv. Geosci.*, *6*, 29–33.

Cai, W., and P. G. Baines (2001), Forcing of the Antarctic circumpolar wave by the El Niño-Southern Oscillation teleconnections, *J. Geophys. Res.*, *106*, 9019–9038.

Cane, M. A., and P. Molnar (2001), Closing of the Indonesian Seaway as a precursor to east African aridification around 3 to 4 million years ago, *Nature*, *411*, 157–162.

Cattle, H., and J. Crossley (1995), Modelling Arctic climate change, *Philos. Trans. R. Soc. London, Ser. A*, *352*, 201–213.

Collins, M. (2000a), The El-Niño Southern Oscillation in the second Hadley Centre coupled model and its response to greenhouse warming, *J. Clim.*, *13*, 1299–1312.

Collins, M. (2000b), Understanding uncertainties in the response of ENSO to greenhouse warming, *Geophys. Res. Lett.*, *27*, 3509–3513.

Collins, M., and The CMIP Modelling Groups (2005), El Niño- or La Niña-like climate change?, *Clim. Dyn.*, *24*, 89–104.

Cox, P., R. Betts, C. Bunton, R. Essery, P. R. Rowntree, and J. Smith (1999), The impact of new land-surface physics on the GCM simulation and climate sensitivity, *Clim. Dyn.*, *15*, 183–203.

Cubash, U., et al. (2001), Projections of future climate change, in *Climate Change 2001: The Scientific Basis: Contribution of Working Group I to the Third Assessment Report of the Intergovernmental Panel on Climate Change (IPCC)*, edited by J. T. Houghton et al., pp. 525–582, Cambridge Univ. Press, New York.

Cusack, S., A. Slingo, J. M. Edwards, and M. Wild (1998), The radiative impact of a simple aerosol climatology on the Hadley Centre GCM, *Q. J. R. Meteorol. Soc.*, *124*, 2517–2526.

Dekens, P. S., D. W. Lea, D. K. Pak, and H. J. Spero (2002), Core top calibration of Mg/Ca in tropical foraminifera: Refining paleotemperature estimation, *Geochem. Geophys. Geosyst.*, *3*(4), 1022, doi:10.1029/2001GC000200.

Dowsett, H. J., and T. M. Cronin (1990), High eustatic sea level during the Middle Pliocene: Evidence from the southeastern U. S. Atlantic coastal plain, *Geology*, *18*, 435–438.

Dowsett, H. J., T. M. Cronin, P. Z. Poore, R. S. Thompson, R. C. Whatley, and A. M. Wood (1992), Micropaleontological evidence for increased meridional heat-transport in the North Atlantic Ocean during the Pliocene, *Science*, *258*, 1133–1135.

Dowsett, H. J., J. A. Barron, R. Z. Poore, R. S. Thompson, T. M. Cronin, S. E. Ishman, and D. A. Willard (1999), Middle Pliocene paleoenvironmental reconstruction: PRISM2, *U.S. Geol. Surv. Open File Rep.*, *99-535*. (Available at http://pubs.usgs.gov/of/1999/of99-535/).

Edwards, J. M., and A. Slingo (1996), Studies with a flexible new radiation code 1: Choosing a configuration for a large-scale model, *Q. J. R. Meteorol. Soc.*, *122*, 689–719.

Fedorov, A. V., P. S. Dekens, M. McCarthy, A. C. Ravelo, P. B. deMenocal, M. Barreiro, R. C. Pacanowski, and S. G. Philander (2006), The Pliocene paradox (mechanisms for a permanent El Niño), *Science*, *312*, 1485–1489.

Gent, P. R., and J. C. McWilliams (1990), Isopycnal mixing in ocean circulation models, *J. Phys. Oceanogr.*, *20*, 150–155.

Gordon, C., C. Cooper, C. A. Senior, H. Banks, J. M. Gregory, T. C. Johns, J. F. B. Mitchell, and R. A. Wood (2000), The simulation of SST, sea ice extents and ocean heat transports in a version of the Hadley Centre coupled model without flux adjustments, *Clim. Dyn.*, *16*, 147–168.

Gregory, J. M., and J. F. B. Mitchell (1997), The climate response to CO_2 of the Hadley Centre coupled AOGCM with and without flux adjustment, *Geophys. Res. Lett.*, *24*, 1943–1946.

Gregory, D., R. Kershaw, and P. M. Inness (1997), Parametrisation of momentum transport by convection II: Tests in single column and general circulation models, *Q. J. R. Meteorol. Soc.*, *123*, 1153–1183.

Harangozo, S. A. (2000), A search for ENSO teleconnections in the west Antarctic Peninsula climate in Austral winter, *Int. J. Climatol.*, *20*, 663–679.

Haug, G. H., and R. Tiedemann (1998), Effect of the formation of the Isthmus of Panama on Atlantic Ocean thermohaline circulation, *Nature*, *393*, 673–676.

Haywood, A. M., and P. J. Valdes (2004), Modelling middle Pliocene warmth: Contribution of atmosphere, oceans and cryosphere, *Earth Planet. Sci. Lett.*, *218*, 363–377.

Haywood, A. M., P. J. Valdes, and B. W. Sellwood (2000), Global scale palaeoclimate reconstruction of the middle Pliocene climate using the UKMO GCM: Initial results, *Global Planet. Change*, *25*, 239–256.

Haywood, A. M., P. Dekens, A. C. Ravelo, and M. Williams (2005), Warmer tropics during the mid-Pliocene? Evidence from alkenone paleothermometry and a fully coupled ocean-atmosphere GCM, *Geochem. Geophys. Geosyst.*, *6*, Q03010, doi:10.1029/2004GC000799.

Held, I. M., S. W. Lyons, and S. Nigam (1989), Transients and the extratropical response to El Niño, *J. Atmos. Sci.*, *46*, 163–174.

Hoerling, M., and A. Kumar (1997), Origins of extreme climate states during the 1982/1983 ENSO winter, *J. Clim.*, *10*, 2859–2870.

Hoskins, B. J., and D. J. Karoly (1981), The steady linear response of a spherical atmosphere to thermal and orographic forcing, *J. Atmos. Sci.*, *38*, 1179–1196.

Huber, M., and R. Caballero (2003), Eocene El Niño: Evidence for robust tropical dynamics in the "Hothouse", *Science*, *299*, 877–881.

Johns, T. C., R. E. Carnell, J. F. Crossley, J. M. Gregory, J. F. B. Mitchell, C. A. Senior, S. F. B. Tett, and R. A. Wood (1997), The second Hadley Centre Coupled Ocean-Atmosphere GCM: Model description, spinup and validation, *Clim. Dyn.*, *13*, 103–134.

Joseph, R., and S. Nigam (2006), ENSO evolution and teleconnections in IPCC's 20th century climate simulations: Realistic representation?, *J. Clim.*, *19*, 4360–4377.

Kerr, R. A. (2005), Climate change: El Niño or La Niña? The past hints at the future, *Science*, *309*, 687.

Kim, S. J., and T. J. Crowley (2000), Increased Pliocene North Atlantic Deep Water: Cause or consequence of Pliocene warming, *Paleoceanography*, *15*, 451–455.

Kürschner, W. M., J. Van der Burgh, H. Visscher, and D. L. Dilcher (1996), Oak leaves as biosensors of late Neogene and early Pleistocene paleoatmospheric CO_2 concentrations, *Mar. Micropaleontol.*, *27*, 299–312.

Latif, M., E. Roeckner, U. Mikolajewicz, and R. Voss (2000), Tropical stabilization of the thermohaline circulation in a greenhouse warming simulation, *J. Clim.*, *13*, 1809–1813.

Levitus, S., and T. P. Boyer (1994), *World Ocean Atlas* 1994, vol. 4, *Temperature*, *NOAA Atlas NESDIS*, vol. 4, 129 pp., NOAA, Silver Spring, Md.

Molnar, P., and M. A. Cane (2002), El Niño's tropical climate and teleconnections as a blueprint for pre-Ice Age climates, *Paleoceanography*, *17*(2), 1021, doi:10.1029/2001PA000663.

Munoz, A., J. Ojeda, and B. Sanchez-Valverde (2002), Sunspot-like and ENSO/NAO-like periodicities in lacustrine laminated sediments of the Pliocene Villarroya Basin (La Rioja, Spain), *J. Paleolimnol.*, *27*(4), 453–463.

Philander, S. G., and A. V. Fedorov (2003), Role of tropics in changing the response to Milankovich forcing some three million years ago, *Paleoceanography*, *18*(2), 1045, doi:10.1029/2002PA000837.

Rasmusson, E. M. (1991), Observational aspects of ENSO cycle teleconnections, in *Teleconnections Linking Worldwide Climate Anomalies*, edited by M. H. Glantz, R. W. Katz, and N. Nicholls, pp. 308–343, Cambridge Univ. Press, New York.

Ravelo, A. C., and D. H. Andreasen (2000), Enhanced circulation during a warm period, *Geophys. Res. Lett.*, *27*, 1001–1004.

Ravelo, A. C., D. H. Andreasen, M. Lyle, A. O. Lyle, and M. W. Wara (2004), Regional climate shifts caused by gradual global cooling in the Pliocene epoch, *Nature*, *42*, 263–267.

Ravelo, A. C., P. S. Dekens, and M. McCarthy (2006), Evidence for El Niño-like conditions during the Pliocene, *GSA Today*, *16*, 4–11.

Raymo, M. E., and G. H. Rau (1992), Plio-Pleistocene atmospheric CO_2 levels inferred from POM $\delta^{13}C$ at DSDP Site 607, *Eos Trans. AGU*, Fall Meet. Suppl., *73*(43), 95.

Raymo, M. E., B. Grant, M. Horowitz, and G. H. Rau (1996), Mid-Pliocene warmth: Stronger greenhouse and stronger conveyor, *Mar. Micropaleontol.*, *27*, 313–326.

Rickaby, R. E. M., and P. Halloran (2005), Cool La Niña during the warmth of the Pliocene?, *Science*, *307*, 1948–1952.

Rind, D., and M. Chandler (1991), Increased ocean heat transports and warmer climate, *J. Geophys. Res.*, *96*, 7437–7461.

Rohling, E. J. (2000), Paleosalinity: Confidence limits and future applications, *Mar. Geol.*, *163*, 1–11.

Rohling, E. J., and G. R. Bigg (1998), Paleosalinity and $\delta^{18}O$: a critical assessment, *J. Geophys. Res.*, *103*, 1307–1318.

Rosenthal, Y., et al. (2004), Interlaboratory comparison study of Mg/Ca and Sr/Ca measurements in planktonic foraminifera for paleoceanographic research, *Geochem. Geophys. Geosyst.*, *5*, Q04D09, doi:10.1029/2003GC000650.

Roulier, L. M., and T. M. Quinn (1995), Seasonal-scale to decadal-scale climatic variability in southwest Florida during the middle Eocene: Inferences from a coralline stable isotope record, *Paleoceanography*, *10*, 429–443.

Ruttlant, J., and H. Fuenzalida (1991), Synoptic aspects of the central Chile rainfall variability associated with the southern oscillation, *Int. J. Climatol.*, *11*, 63–76.

Schmidt, G. A. (1998), Oxygen-18 variations in a global ocean model, *Geophys. Res. Lett.*, *25*, 1201–1204.

Schmidt, G. A. (1999), Forward modelling of carbonate proxy data from planktonic foraminifera using oxygen isotope tracers in a global ocean model, *Paleoceanography*, *14*, 482–497.

Shackleton, N. J., J. Le, A. Mix, and M. A. Hall (1992), Carbon isotope records from Pacific surface waters and atmospheric carbon dioxide, *Quat. Sci. Rev.*, *11*, 387–400.

Thorpe, R. B., J. M. Gregory, T. C. Johns, R. A. Wood, and J. F. B. Mitchell (2001), Mechanisms determining the Atlantic Thermohaline Circulation response to greenhouse gas forcing in a non-flux adjusted coupled climate model, *J. Clim.*, *14*, 3102–3116.

Turner, J. (2004), The El Niño Southern Oscillation and Antarctica, *Int. J. Climatol.*, *24*, 1–31.

Van der Burgh, J., H. Visscher, D. L. Dilcher, and W. M. Kürschner (1993), Paleoatmospheric signatures in Neogene fossils leaves, *Science*, *260*, 1788–1790.

Wara, M. W., A. C. Ravelo, and M. L. Delaney (2005), Permanent El Niño–like conditions during the Pliocene warm period, *Science*, *309*, 758–761.

White, W. B., and R. G. Peterson (1996), An Antarctic circumpolar wave in surface pressure, wind, temperature and sea-ice extent, *Nature*, *380*, 699–702.

Williams, K. D., C. A. Senior, and J. F. B. Mitchell (2001), Transient climate change in the Hadley Centre models: The role of physical processes, *J. Clim.*, *14*, 2659–2674.

Zachos, J. C., L. D. Stott, and K. C. Lohmann (1994), Evolution of early Cenozoic marine temperatures, *Paleoceanography*, *9*, 353–387.

A. M. Haywood, School of Earth and Environment, University of Leeds, Environment Building, Leeds LS2 9JT, UK. (ahay@bas.ac.uk)

V. L. Peck, Geological Sciences Division, British Antarctic Survey, High Cross, Madingley Road, Cambridge CB3 0ET, UK.

P. J. Valdes, School of Geographical Sciences, University of Bristol, University Road, Bristol BS8 1SS, UK.